Capability of TEC correlation analysis and deceleration at propagation velocities of MSTID: Preseismic ionospheric anomalies before the large earthquakes

Ken Umeno[1,1], Ryo Nakabayashi[1,1], Takuya Iwata[1,1], and Minghui Kao[2,2]

[1]Kyoto University
[2]

November 30, 2022

Abstract

Capability of TEC 's CoRrelation Analysis (CRA) (Iwata and Umeno, 2016) for detecting preseismic anomaly is explained from the view point of the increase in signal-to-noise ratio to {\it amplify} preseismic TEC's small anomaly signals with multiple sensor data synchronization and correlation to respond to all the criticisms proposed recently by Ikuta et al. 2021. Furthermore, deceleration at propagation velocities of MSTID before the 2016 Kumamoto earthquake firstly observed by CRA as velocity reduction of MSTID propagation in the F Layer of the ionosphere is then elucidated as a candidate of preseismic anomalies. This paper presents three models to explain its physical relationship with preseismic anomalies before large earthquakes. In particular, Model 1 predicts that the 35 m/s change in MSTID propagation velocities estimated by TEC's CRA requires $0.58*10^{-3}$ V/m electric field change in the F Layer ionosphere, which is almost consistent with the estimation (Kelley et. al. 2017) in that the $E*B/B^2$ rift of 12 m/s for dislocations of electrons requires $0.5*10^{-3}$ V/m electric field in the E Layer to explain Heki's finding of TEC anomaly behavior before the Tohoku-Oki earthquake. The (10000) times amplified effect of weak signals such as 0.58 mV/m in electrical field to affect MSTID propagation velocity change as is firstly observed by Iwata and Umeno, 2017 by CRA which has significant amplified capability. Contrary to the claim by Ikuta et al. 2021, TEC's correlation anomalies detected (Iwata and Umeno 2016 and 2017) already provided supporting evidences that physical preseismic anomalies really exist.

Capability of TEC correlation analysis and deceleration at propagation velocities of MSTID: Preseismic ionospheric anomalies before the large earthquakes

Ken Umeno[1], Ryo Nakabayashi[1], Takuya Iwata[1], Minghui Kao[1]

[1]Department of Applied Mathematics and Physics, Graduate School of Informatics, Kyoto University, Kyoto, Japan

Key Points:

- Capability of TEC 's CoRrelation Analysis (CRA) (Iwata and Umeno, 2016) for detecting preseismic anomaly is explained with additional data analysis to respond to all the criticisms proposed recently by Ikuta et al. 2021.
- Deceleration at propagation velocities of Medium-Scale Traveling Ionospheric Disturbances (MSTID) before the 2016 Kumamoto earthquake firstly observed by CRA (Iwata and Umeno, 2017) is elucidated as a candidate of preseismic (physical) anomaly by presenting three physical models (Models 1-3) together with additional CRA analysis.
- According to Model 1, velocity change of 35 m/s of MSTID propagation estimated by TEC's CRA requires an electric field change of 0.58×10^{-3} V/m in the F Layer ionosphere, which is almost consistent with the estimation (Kelley et. al. 2017) in that $\boldsymbol{E} \times \boldsymbol{B}/B^2$ drift of 12 m/s for dislocations of electrons requires an electric field change of 0.5×10^{-3} in the E Layer.

Corresponding author: Ken Umeno, `umeno.ken.8z@kyoto-u.ac.jp`

Abstract

Capability of TEC 's CoRrelation Analysis (CRA) (Iwata and Umeno, 2016) for detecting preseismic anomaly is explained from the view point of the increase in signal-to-noise ratio to *amplify* preseismic TEC's small anomaly signals with multiple sensor data synchronization and correlation to respond to all the criticisms proposed recently by Ikuta et al. 2021.

Furthermore, deceleration at propagation velocities of MSTID before the 2016 Kumamoto earthquake firstly observed by CRA (Iwata and Umeno, 2017) as velocity reduction of MSTID propagation in the F Layer of the ionosphere is then elucidated as a candidate of preseismic anomalies. This paper presents three models to explain its physical relationship with preseismic anomalies before large earthquakes. In particular, Model 1 predicts that the 35 m/s change in MSTID propagation velocities estimated by TEC's CRA requires 0.58×10^{-3} V/m electric field change in the F Layer ionosphere, which is almost consistent with the estimation (Kelley et. al. 2017) in that the $\boldsymbol{E} \times \boldsymbol{B}/B^2$ drift of 12 m/s for dislocations of electrons requires 0.5×10^{-3} V/m electric field in the E Layer to explain Heki's finding of TEC anomaly behavior before the Tohoku-Oki earthquake. The 10000 times amplified effect of weak signals such as 0.58 mV/m in electrical field to affect MSTID propagation velocity change as is firstly observed by Iwata and Umeno, 2017 by CRA which has significant amplified capability.

Contrary to the claim by Ikuta et al. 2021, TEC's correlation anomalies detected (Iwata and Umeno 2016 and Iwata and Umeno 2017) already provided supporting evidences that physical preseismic anomalies really exist.

1 Introduction

CorRelation Analysis (CRA, hereafter) is a general method to extract signal from complicated noise in diverse kinds of signal processing. It can be distant to merge radio signals of Quasars to lock and unlock digital communication as an encryption tool, or is near to extract Wi-Fi signal from noise of home appliances around people's daily living. CRA to detect total electron content (TEC) anomalies before large earthquakes is based on the very long baseline interferometry's concept and spreading spectrum communications technology. It has been implemented to report in 2016, Iwata and Umeno, https://doi.org/10.1002/2016JA023036 (hereafter I&U16), 2017, Iwata and Umeno, https://doi.org/10.1002/2017JA023921 (hereafter I&U17), and 2019, Goto, et al., https://doi.org/10.1029/2019JA026640 (hereafter Goto et al.19).

Those are sequentially targeted in the 2011 Tohoku Oki earthquake (Mw9.0, depth 24km), the 2016 Kumamoto earthquake (Mw7.3, depth 12km), and the 2016 Tainan earthquake (Mw6.4, depth 14.6km) respectively. Recently, Ikuta, Oba, Kiguchi and Hisada (2021, Ikuta et al., a preprint; hereafter Ikuta et al. 21) examined the results of I&U16 and I&U17 by the statistical analysis and posed a question on the CRA capability on detecting preseismic anomaly. The existence of preseismic TEC anomalies before large earthquakes has been debated until today (Heki 2011, Kamogawa-Kakinami 2013, Heki-Enomoto 2013, Masci et al. 2015, Kelly et al. 2017, Muafiry and Heki 2020, Eisenbeis and Occipinti 2021). Such debate for decade is caused by lacking of *conclusive* physical models to explain preseismic TEC anomalies. The purpose of the present paper is to respond to Ikuta et al. 21 on the above issue by adding an evidence to support that TEC correlation anomalies detected in I&U16 and I&U17 are really physical preseismic anomalies. The TEC CRA capability on detecting preseismic behavior will be discussed in the this paper. The general characteristics of CRA is introduced in Section 2. Three physical models showing TEC

72 correlation anomalies in I&U17 will also be presented to show that the 35 m/s change
73 at deceleration at the propagation velocities of MSTID detected by CRA requires
74 the 0.58 mV/m electric field in the ionosphere in Section 3. Supportive data anal-
75 ysis of CRA will be presented in Section 4. Discussion about the data analysis to
76 respond to the analysis of Ikuta et al. 21 and concluding remarks will be presented
77 in Section 5.

78 2 Signal-to-Noise Ratio in CoRrelation Analysis (CRA)

79 To sense anomalies from GNSS stations, CRA computes a correlation among
80 abnormalities observed at GNSS stations. The first step of CRA is to choose a GNSS
81 station to correlate. Once we choose a central station, $M(\geq 1)$ surrounding stations,
82 which are the nearest to the central station, can be selected. One can number the
83 central station and each surrounding stations from 0 to M, where the number 0
84 means the central station and the numbers 1 to M are allocated to the surround-
85 ing stations. Let $X_{i,t}$ be abnormalities of the station i at time t such as prediction
86 errors computed from sample data at the station i. Let t_s be the time length of sam-
87 ple data for learning to predict which were set to 2.0 hours in the CRA in I&U16,
88 I&U17 and Goto et al. 19.

The crux of the CoRrelation Analysis (CRA) (I&U16) is to compute a correla-
tion given by

$$C(T) = \frac{1}{NM} \sum_{i=1}^{M} \sum_{j=0}^{N-1} X_{0,t+t_S+j\Delta t} \cdot X_{i,t+t_S+j\Delta t} \tag{1}$$

$$T = t + t_S + t_{test},$$

where $N(> 1)$ is the number of data in a Test Data during the time $t + t_S$ to $t + t_S + t_{test}$, Δt is a sampling interval in the Test Data (usually 30 seconds for TEC data), t_S is the time length of the Sample Data (Learning period) and t_{test} is the time length of the Test Data (Prediction Period). I&U16 and I&U17 set up that $t_S = 2.0$[hours] and $t_{test} = 0.25$[hours] . The correlation value $C(T)$ can be rewritten as:

$$C(T) = \frac{1}{N} \sum_{j=0}^{N-1} X_{0,t+t_S+j\Delta t} \cdot \left(\frac{1}{M} \sum_{i=1}^{M} X_{i,t+t_S+j\Delta t} \right) = \frac{1}{N} \sum_{j=0}^{N-1} X_{0,t+t_S+j\Delta t} \cdot \tilde{X}_{0,t+t_S+j\Delta t},$$

where

$$\tilde{X}_{0,t+t_S+j\Delta t} = \frac{1}{M} \sum_{i=1}^{M} X_{i,t+t_S+j\Delta t}.$$

Note that if $M = 1$, $C(T)$ becomes just a normal correlation between X_0 and X_i:

$$C(T) = \frac{1}{N} \sum_{j=0}^{N-1} X_{0,t+t_S+j\Delta t} \cdot X_{i,t+t_S+j\Delta t}.$$

Thus, from the above equation, one can see that $C(T)$ can capture a *synchronized temporal anomaly patterns* correlated between X_0 (a value at the central station) and $\tilde{X}_0$ (a mean value of the values X_i). If anomaly patterns of observational points are coherently periodic such as medium-scale traveling disturbances (MSTIDs), $C(T)$ also shows periodic patterns with the same period. On the contrary, if anomaly patterns are coherently non-periodic irregular patterns, $C(T)$ also show a certain irregular pattern. Thus, not only its value $C(T)$, but also a *temporal characteristics* of $C(T)$ are vitally important to elucidate anomaly alert. If N is large, the following relation

$$\sum_{j=0}^{N-1} X_{0,t+t_S+j\Delta t} \cdot \tilde{X}_{0,t+t_S+j\Delta t} = O(\sqrt{N})$$

holds for non-correlated noisy signals X_0 and X_i from the central limit theorem (CLT). Thus,

$$C(T) = \frac{1}{N} \sum_{j=0}^{N-1} X_{0,t+t_S+j\Delta t} \cdot \tilde{X}_{0,t+t_S+j\Delta t} = O\left(\frac{1}{\sqrt{N}}\right) \to 0 \quad \text{for } N \to \infty. \quad (2)$$

On the contrary, for some coherent synchronized signals X_0 and X_i due to some anomaly phenomena, it is evident that

$$\sum_{j=0}^{N-1} X_{0,t+t_S+j\Delta t} \cdot \tilde{X}_{0,t+t_S+j\Delta t} = O(N).$$

Thus we can expect a higher C(T) such that

$$|C(T)| = \left| \frac{1}{N} \sum_{j=0}^{N-1} X_{0,t+t_S+j\Delta t} \cdot \tilde{X}_{0,t+t_S+j\Delta t} \right| = O(1) > 0 \quad \text{for } N \to \infty, \quad (3)$$

which clearly distinguish a signal from noisy signals when N is sufficiently large. An SNR or signal-to-noise ratio at this abnormality detector $C(T)$ can be measured by the ratio between the variances of signal and noise; thus the following general relation holds:

$$\text{SNR} = \frac{(O(1))^2}{\left(O\left(\frac{1}{\sqrt{N}}\right)\right)^2} = O(N).$$

Thus, N is a key parameter of CRA to measure temporal correlations with each temporal abnormalities, where N is regarded as the spreading factor in spread spectrum technology.

3 Deceleration of propagation velocities of MSTID and the physical mechanism

In this section a general relation between the deceleration at propagation velocities in MSTID and a change of electric field strength in the ionosphere is derived to provide a physical basis to the anomaly patterns detected by CRA. Physical behavior of MSTID can be understood in terms of plasma physics (physics for ionized gases) (Spitzer, 1962).

The equations of motion for electrons of mass m_e and ions of mass m_i in the ionosphere are given by

$$n_e m_e \left(\frac{\partial \boldsymbol{v}_e}{\partial t} + (\boldsymbol{v}_e \cdot \nabla)\boldsymbol{v}_e \right) = n_e m_e \boldsymbol{g} - e n_e (\boldsymbol{E} + \boldsymbol{v}_e \times \boldsymbol{B}) - \nabla p_e - n_e m_e \nu_{en}(\boldsymbol{v}_e - \boldsymbol{v}_n) + \sum_i \boldsymbol{R}_{ie} \quad (4)$$

$$n_i m_i \left(\frac{\partial \boldsymbol{v}_i}{\partial t} + (\boldsymbol{v}_i \cdot \nabla)\boldsymbol{v}_i \right) = n_i m_i \boldsymbol{g} + e Z_i n_i (\boldsymbol{E} + \boldsymbol{v}_i \times \boldsymbol{B}) - \nabla p_i - n_i m_i \nu_{in}(\boldsymbol{v}_i - \boldsymbol{v}_n) - \boldsymbol{R}_{ie} - \sum_{j \neq i} \boldsymbol{R}_{ij}, \quad (5)$$

where $\boldsymbol{v}_e(\boldsymbol{v}_i)$ is the velocity of an electron (an ion i), Z_i is the ion charge number (multiples of e) of ion i, $n_e(n_i)$ is the number density of electrons (ions i), $\nu_{en}(\nu_{in})$ is the frequency of collisions between an electron (an ion i) and neutral particles, $\nabla p_e(\nabla p_i)$ is the gradient of pressure acting on electrons (ions i), $\boldsymbol{R}_{ie}$ is the force per unit volume affected by collisions between electrons and ions i, $\boldsymbol{R}_{ij}$ is the force per unit volume affected by collisions between ions i and another kind of ions j and $\boldsymbol{g}$ the gravity force affected by the earth is a vector per unit mass per unit volume. After summing Eq. (4) and $\sum_i$ Eq. (5), with $\sum_i \boldsymbol{R}_{ie}$(in Eq. (4))$+\sum_i -\boldsymbol{R}_{ie}$(in Eq. (5)) = 0 and $\sum_i \sum_{j \neq i} \boldsymbol{R}_{ij} = 0$, one can derive the plasma equation:

$$\rho \frac{\partial \boldsymbol{v}}{\partial t} + n_e m_e (\boldsymbol{v}_e \cdot \nabla)\boldsymbol{v}_e + \sum_i n_i m_i (\boldsymbol{v}_i \cdot \nabla)\boldsymbol{v}_i = \rho \boldsymbol{g} + \boldsymbol{j} \times \boldsymbol{B} - \nabla p - \sum_i n_i m_i \nu_{in}(\boldsymbol{v}_i - \boldsymbol{v}_n),$$

where $\rho(\equiv n_e m_e + \sum_i n_i m_i)$ is the mass density, $\boldsymbol{v}(\equiv (n_e m_e \boldsymbol{v}_e + \sum_i n_i m_i \boldsymbol{v}_i)/\rho)$ is the center of mass velocity, $\boldsymbol{j}(\equiv -e(n_e \boldsymbol{v}_e - \sum_i Z_i n_i \boldsymbol{v}_i))$ is the current density, and $p(\equiv p_e + p_i)$ is the pressure (plasma pressure). Here, by electrical neutrality of plasma, $\sum_i n_i Z_i = n_e$ and we neglect the term $-n_e m_e \nu_{en}(\boldsymbol{v}_e - \boldsymbol{v}_n)$ because the electron cyclotron frequency $\Omega_e = \dfrac{eB}{m_e}$ is much greater than the collision frequency ν_{en} and $m_e \ll m_i$. The layer of the ionosphere for considering MSTID is the F-Layer with the 300km height above the ground. In this case, one can safely assume that ions in that layer are of one type, O^+ for simplicity . Thus, $\rho \simeq n_i m_i$ and $\boldsymbol{v}_i \simeq \boldsymbol{v}$ hold because $m_e \ll m_i$. Furthermore,

$$n_e m_e (\boldsymbol{v}_e \cdot \nabla)\boldsymbol{v}_e + \sum_i n_i m_i (\boldsymbol{v}_i \cdot \nabla)\boldsymbol{v}_i \simeq \rho \frac{D\boldsymbol{v}}{Dt},$$

where $\dfrac{D\boldsymbol{v}}{Dt} \equiv \dfrac{\partial \boldsymbol{v}}{\partial t} + (\boldsymbol{v} \cdot \nabla)\boldsymbol{v}$. Accordingly, the final form of the equation motion for ionized gas (ionosphere) above the 300km is:

$$\rho \frac{D\boldsymbol{v}}{Dt} = \rho \boldsymbol{g} + \boldsymbol{j} \times \boldsymbol{B} - \nabla p - n_i m_i \nu_{in}(\boldsymbol{v}_i - \boldsymbol{v}_n). \tag{6}$$

An ionospheric current $\boldsymbol{j}_\perp$ perpendicular to Earth's magnetic field line $\boldsymbol{B}$ penetrating the ionosphere is given by

$$\boldsymbol{j}_\perp = \sigma_P (\boldsymbol{E}_\perp + \boldsymbol{v}_n \times \boldsymbol{B}) + \sigma_H \frac{\boldsymbol{B}}{B} \times (\boldsymbol{E}_\perp + \boldsymbol{v}_n \times \boldsymbol{B}),$$

where $\boldsymbol{E}_\perp$ is an electric field vector perpendicular to $\boldsymbol{B}$, $\boldsymbol{v}_n$ is the mean velocity vector of a gas of neutral particles, σ_P is thePedersen conductivity computed by $\sigma_P = \dfrac{n_i e}{B}\left(\dfrac{\nu_{in}\Omega_i}{\nu_{in}^2 + \Omega_i^2} + \dfrac{\nu_{en}\Omega_e}{\nu_{en}^2 + \Omega_e^2}\right)$ and σ_H is the Hall current conductivity computed by $\sigma_H = \dfrac{n_i e}{B}\left(\dfrac{\Omega_i^2}{\nu_{in}^2 + \Omega_i^2} - \dfrac{\Omega_e^2}{\nu_{en}^2 + \Omega_e^2}\right)$ (Maeda, 1977). In the F-Layer ionosphere 300km over the earth, $\sigma_P \gg \sigma_H$. Thus one can safely assume that $\boldsymbol{j}_\perp = \sigma_P (\boldsymbol{E}_\perp + \boldsymbol{v}_n \times \boldsymbol{B})$. The obtained equation of motion for a velocity $\boldsymbol{v}_\perp$ perpendicular to the geomagnetic field $\boldsymbol{B}$ is:

$$\frac{D\boldsymbol{v}_\perp}{Dt} = \boldsymbol{g}_\perp + \frac{e}{m_i B}\left(\frac{\nu_{in}\Omega_i}{\nu_{in}^2 + \Omega_i^2} + \frac{\nu_{en}\Omega_e}{\nu_{en}^2 + \Omega_e^2}\right)(\boldsymbol{E}_\perp + \boldsymbol{v}_n \times \boldsymbol{B}) \times \boldsymbol{B} - \frac{(\nabla p)_\perp}{n_i m_i} - \nu_{in}(\boldsymbol{v}_{i\perp} - \boldsymbol{v}_{n\perp}).$$

Propagation $\boldsymbol{v}_\perp$ of MSTID is essentially a *macroscopically stationary drift* motion of an ionized gas (not electrons). Thus, the propagation velocity of MSTID satisfies the continuity equation for an incompressible fluid:

$$\frac{\partial \rho}{\partial t} + \nabla \cdot (\rho \boldsymbol{v}) = 0 \text{ with } \nabla \cdot \boldsymbol{v} = 0 \Rightarrow \frac{D\boldsymbol{v}}{Dt} = \frac{D\boldsymbol{v}_\perp}{Dt} = 0.$$

Therefore, we get the propagation velocity of MSTID which is the perpendicular to $\boldsymbol{B}$ by the following formula:

$$\boldsymbol{v}_\perp = \boldsymbol{v}_{n\perp} + \frac{\boldsymbol{g}_\perp}{\nu_{in}} + \frac{e}{m_i B}\left(\frac{\Omega_i}{\nu_{in}^2 + \Omega_i^2} + \frac{\nu_{en}\Omega_e}{\nu_{in}(\nu_{en}^2 + \Omega_e^2)}\right)(\boldsymbol{E}_\perp + \boldsymbol{v}_n \times \boldsymbol{B}) \times \boldsymbol{B} - \frac{(\nabla p)_\perp}{\nu_{in} n_i m_i}. \tag{7}$$

Suppose an electric field $\boldsymbol{E}_\perp$ is changed as $\boldsymbol{E}_\perp \to \boldsymbol{E}_\perp - \boldsymbol{\Delta E}_\perp$. Such a change in $\boldsymbol{E}_\perp$ also changes the propagation velocity of MSTID as $\boldsymbol{v}_\perp \to \boldsymbol{v}_\perp - \boldsymbol{\Delta v}_\perp$ where

$$\boldsymbol{\Delta v}_\perp = \frac{e}{m_i}\left(\frac{\Omega_i}{\nu_{in}^2 + \Omega_i^2} + \frac{\nu_{en}\Omega_e}{\nu_{in}(\nu_{en}^2 + \Omega_e^2)}\right)\boldsymbol{\Delta E}_\perp \times \frac{\boldsymbol{B}}{B}. \tag{8}$$

Finally, one can obtain:

$$\Delta v_\perp = \frac{\sigma_P B}{n_i m_i \nu_{in}}\Delta E_\perp = \frac{e}{m_i}\left(\frac{\Omega_i}{\nu_{in}^2 + \Omega_i^2} + \frac{\nu_{en}\Omega_e}{\nu_{in}(\nu_{en}^2 + \Omega_e^2)}\right)\Delta E_\perp \simeq \frac{e}{m_i \Omega_i}\Delta E_\perp \tag{9}$$

99   which is the causal relation between the *deceleration* at propagation velocities of
100 MSTID ($\Delta v_\perp$) and $\Delta E_\perp$, a sudden change of electric field in the ionosphere.

Namely, a sudden change in the opposite direction (in the eastward direction at
the midnight, see Figure 1.) causes deceleration at MSTID's propagation velocities
(Model 1). Here one can assume that $\Omega_i \simeq 100$ rad s^{-1} for quantitative validation of
the model. Note that $e = 1.602 \times 10^{-19}$ C, $m_p = 1.673 \times 10^{-27}$ kg, $m_i = 16\ m_p$. In
this case, $\Delta v_\perp = 35$ m$\cdot$s^{-1} change with the deceleration at propagation velocities in
MSTID requires $\Delta E_\perp = 0.58 \times 10^{-3}$ N$\cdot$C$^{-1} = 0.58$ mV/m change in the F Layer
of the ionosphere. Thus, even a small change in electric field in the F layer can be
measured by a macroscopic data estimation of *deceleration at propagation velocities
of MSTID*. In other words, even a fairly small change in the electric field strength
can be measured by *amplified effect* with the propagation velocity of MSTID by the
following formula:

$$a \equiv \frac{\Delta v_\perp}{\Delta E_\perp} = \text{Const.} = \frac{eZ}{m_i \Omega_i} = 5.9848 \times 10^4 \text{ m} \cdot \text{C} \cdot \text{s}^{-1} \cdot \text{N}^{-1} \simeq 6 \times 10^4 \text{ T}^{-1},$$

where a is an *amplification factor* between $\Delta v_\perp$ and $\Delta E_\perp$ and can be regarded as a
constant parameter. It is of interest to note that our estimation such that 35 m$\cdot$s^{-1}
change in the propagation velocities of MSTID requires 0.58×10^{-3} N$\cdot$C^{-1} electric
field lines at 300km height is almost consistent with Kelley et. al. 2017 's estimation
(Kelley et. al. 2017) such that an $\boldsymbol{E} \times \boldsymbol{B}/B^2$ drift of 12m$\cdot$s^{-1} for the dislocation of
electrons observed with TEC and its 3D-tomography analysis by Heki et. al. (Heki,
2011; Muafiry and Heki, 2020; Heki, 2021) requires 0.5×10^{-3}N$\cdot$C^{-1} electric field
lines at the base of ionosphere, although the above two estimation methods are *to-
tally different*. Responsible components of plasma in MSTID propagation are *ions* as
$\rho \simeq m_i n_i$ in the F region while Heki 2011 and Kelley et. al. 2017 consider a model
of *electron* dislocations due to an $\boldsymbol{E} \times \boldsymbol{B}/B^2$ drift in the E region. Other physical
models responsible for MSTID's deceleration at propagation velocities can be at-
tributed to a *reduction of Pedersen conductivity* σ_P such as $\sigma_P \rightarrow \sigma_P - \Delta \sigma_P$ by

$$\Delta v_\perp = \frac{\Delta \sigma_P B}{n_i m_i \nu_{in}} E_\perp \quad \text{(Model 2)} \tag{10}$$

or an *increase in ion density* as $n_i \rightarrow n_i + \Delta n_i$ with $\Delta n_i > 0$ by

$$\Delta v_\perp = -\frac{\sigma_P \Delta n_i B}{n_i^2 m_i \nu_{in}} E_\perp + \frac{(\nabla p)_\perp \Delta n_i}{n_i^2 m_i \nu_{in}} \simeq -\frac{\sigma_P \Delta n_i B}{n_i^2 m_i \nu_{in}} E_\perp \quad \text{(Model 3)} \tag{11}$$

101 where we have safely discard the term of the gradient of pressure during the time
102 scale of preservation of the MSTID periodic stripe structure. Koyama et. al. 2019
103 (Koyama et. al., 2019) observed the reduction of Pedersen conductivity prior to the
104 2011 Tohoku-oki earthquake, which is consistent with Model 2 (the former theory
105 on a reduction of Perdersen conductivity of the F region). They observed the *en-
106 hancement* of O$^+$ by DMSP satellites prior to the 2011 Tohoku-Oki earthquake,
107 which is also consistent with Model 3 (the latter theory on an increase of ion den-
108 sity) (Oyama et. al., 2019). Figure 1 summarizes the three physical models pre-
109 sented here where MSTID at the midnight hour of the mid-latitude northern hemi-
110 sphere is assumed.

4   Supporting evidence for deceleration of propagation velocities at MSTID before the 2016 Kumamoto earthquake

114 We analyzed GNSS data obtained by GEONET and then converted them to
115 get Slant TEC data to perform CRA as (I&U16, I&U17). We selected the 15 GNSS
116 stations located in Kyushu island in Japan as the central stations (See Figure S1.)
117 and set the same parameter as $M = 30$ as I&U16, and I&U17. Figure 2 and 3 show
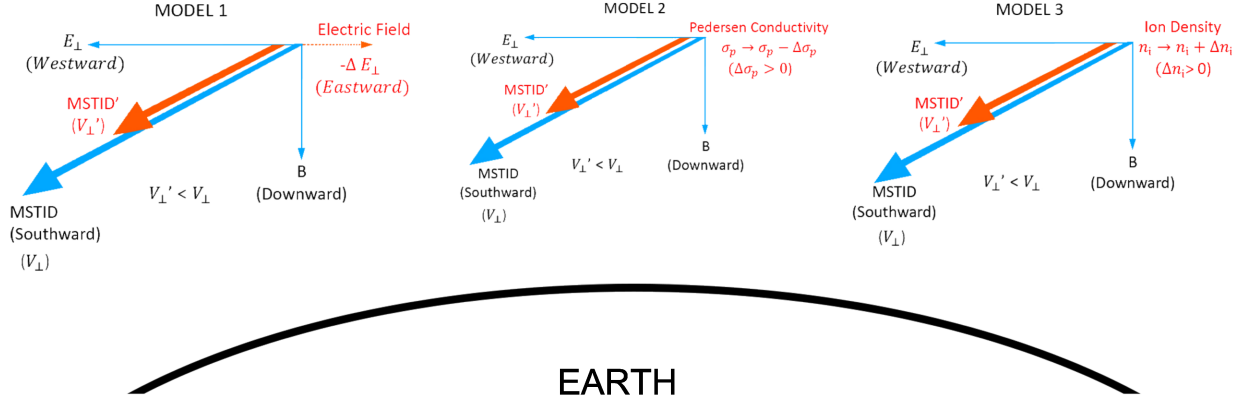
Figure 1. Physical Models for Deceleration at Propagation Velocities of MSTID
Three physical models (Models 1 to 3) explaining deceleration at propagation velocities
with MSTID at the midnight hour are depicted.

**Table 1.** Half Periods of MSTID on April 15, 2016 Estimated by CRA

Station	ΔT_1 (hour)	ΔT_2 (hour)	Ratio $\gamma \left(\equiv \dfrac{\Delta T_1}{\Delta T_2} \right)$	t_1 (UTC)	t_2 (UTC)	t_3 (UTC)
0087	0.192	0.283	0.676	15.358	15.550	15.833
0089	0.233	0.317	0.737	15.258	15.492	15.808
0451	0.200	0.292	0.686	15.367	15.567	15.858
0452	0.217	0.325	0.667	15.292	15.508	15.833
0453	0.208	0.292	0.714	15.383	15.592	15.883
0685	0.183	0.308	0.595	15.308	15.492	15.800
0687	0.200	0.308	0.649	15.292	15.492	16.800
0688	0.208	0.308	0.676	15.333	15.541	15.850
0710	0.233	0.317	0.737	15.283	15.517	15.833
0771	0.208	0.292	0.7143	15.400	15.608	15.900
1060	0.183	0.300	0.611	15.300	15.483	15.783
1062	0.200	0.292	0.686	15.392	15.592	15.883
1063	0.200	0.308	0.649	15.325	15.525	15.833
1064	0.233	0.325	0.718	15.233	15.467	15.791
1069	0.150	0.267	0.563	15.200	15.350	15.617

that MSTID deceleration at propagation velocities is clearly seen. On the earth-quake day, the half periods ΔT_1 and Δ_2 of the MSTID one cyclic period became widen as $\Delta T_1 < \Delta T_2$ while the MSTID maintains the spatial periodic stripe structure with the wave length Λ. See Figure S2 and S3 for the MSTID spatial structures on the corresponding days.

Thus, the averaged values over the 15 stations depicted in Fig. S1 are obtained as:

$$\overline{\Delta T_1} = 0.203 \text{ hour}, \ \overline{\Delta T_2} = 0.302 \text{ hour}, \ \overline{\gamma} \equiv \overline{\frac{\Delta T_1}{\Delta T_2}} = 0.617.$$

The wave length Λ of MSTID around 15:50 (UTC) on April 15, 2016 is estimated as $\Lambda = 1577160$ m. by CRA with all the GNSS stations in Japan (See Figure S2).
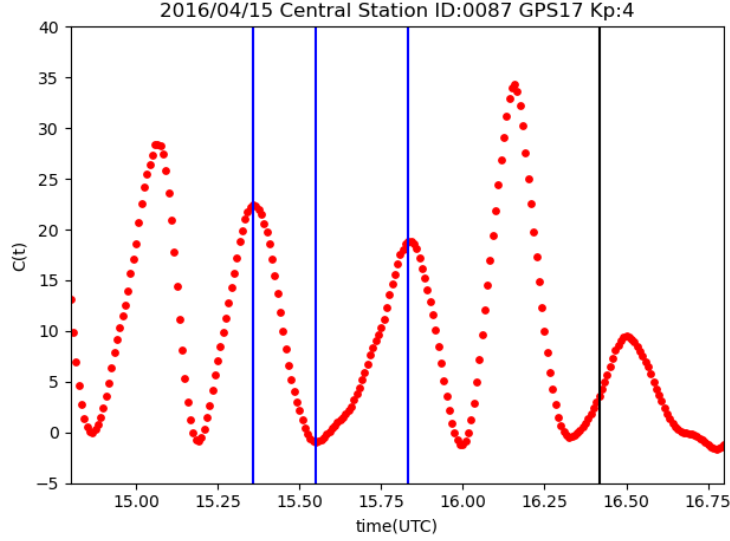
Figure 2. Correlation values (0087) before the 2016 Kumamoto earthquake The vertical axis shows the correlation $C(T)$ and the horizontal one the time t (UTC). The black line indicates the exact time 16:25 (UTC) when the 2016 Kumamoto earthquake occurred. The blue lines indicate the times t_1, t_2, t_3, $(t_1 < t_2 < t_3)$ when $C(T)$ has extremal values. Because $0 < \Delta T_1 \equiv t_2 - t_1 < \Delta T_2 \equiv t_3 - t_2$, a deceleration at propagation velocity of MSTID is clarified. The GNSS station 0087 (Koga, Fukuoka Prefecture) is used as the central station and the GPS satellite RRN17 is selected for the analysis.

Thus, we obtain the propagation velocities of MSTID:

$$v(\text{before}) = \frac{\Lambda}{2\overline{\Delta T_1}} = 107.658 \text{ m} \cdot \text{s}^{-1}, \ v(\text{after}) = \frac{\Lambda}{2\overline{\Delta T_2}} = 72.431 \text{ m} \cdot \text{s}^{-1}.$$

A deceleration Δv at MSTID propagation velocities is finally obtained by

$$\Delta v = v(\text{before}) - v(\text{after}) = \frac{\Lambda}{2} \left(\frac{1}{\Delta T_1} - \frac{1}{\Delta T_2} \right) = 35.23 \text{ m} \cdot \text{s}^{-1}.$$

On the contrary, the data on April 13, 2016 where the usual MSTID was identified by I&U17 shows the opposite sign: no deceleration at propagation velocities in MSTID is observed. As can be seen in Figs. 3-4, the half periods Δ_1 and Δ_2 on April 13, 2016 are almost same $\gamma = \frac{\Delta_1}{\Delta_2} \simeq 1$. Through the remarkable difference between the deceleration of MSTID on the earthquake day (April 15,2016) and non-deceleration of MSTID on April 13, 2016 as also seen in Fig. S2 and S3, one can consider a deceleration at propagation velocities at MSTID is the *characteristics of preseismic phenomena* because it is extremely difficult to find such a deceleration at MSTID propagation velocity on the usual MSTIDs (Otsuka 2011). Moreover, such a phenomenon as a deceleration at MSTID propagation velocities is a single event anomaly. Thus, the statistical approach of MSTID propagation velocities discussed by Ikuta et al. 21 is not adequate for evaluating CRA capability of detecting pre-seismic anomalies. The other twenty six figures, Figures S4 to S29 also support that a deceleration of propagation velocities of MSTID occurred on the earthquake day while such a deceleration was not observed on the non-earthquake day. We conclude here that the TEC's correlation analysis presented here shows the deceleration at
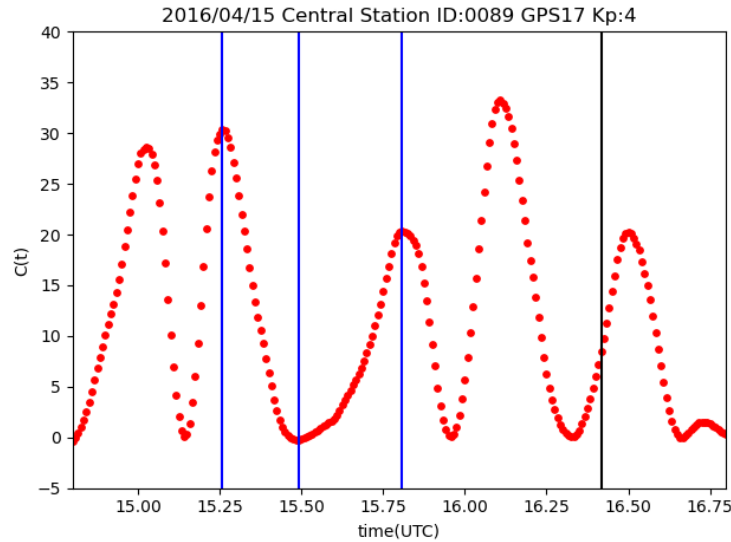
Figure 3. Correlation values (0089) before the 2016 Kumamoto earthquake on April 15, 2016 The vertical axis shows the correlation $C(T)$ and the horizontal one the time t (UTC). The black line indicates the exact time 16:25 (UTC) when the 2016 Kumamoto earthquake occurred. The blue lines indicate the times t_1, t_2, t_3, $(t_1 < t_2 < t_3)$ when $C(T)$ has extremal values. Because $0 < \Delta T_1 \equiv t_2 - t_1 < \Delta T_2 \equiv t_3 - t_2$, a deceleration at propagation velocity of MSTID is clarified. The GNSS station 0089 is used as the central station and the GPS satellite RRN17 is selected for the analysis.

propagation velocities of MSTID and its physical existence on the deceleration of MSTID propagation velocities before the 2016 Kumamoto earthquake is conclusive by CRA.

5 Discussion and Concluding Remarks

A preseismic ionospheric anomaly, if it exists, should be distinguished from other space weather phenomena such as MSTID and high geomagnetic activity. For the issue on distinction between ionospheric anomaly and MSTID, Ikuta et al. 21 argues that the 65-168 m/s MSTID propagation velocity range of I&U17 is not abnormally low as compared to the statistics on the propagation velocities reported in the past (Otsuka, 2011) and Ikuta et al. concluded that TEC anomaly detected for the 2016 earthquake day is not a preseismic one. We argue that this kind of anomaly reported on I&U17 is not a statistical anomaly but a *single event anomaly* (focus on both time and space). There has been high $C(T)$ computed by feeding two hours training data period. Thus such a simple statistical argument on the judgement about the capability of CRA and an existence of preseismic anomaly is not enough and not conclusive. With additional data analysis with the half periods of MSTID obtained by CRA in the preceding section, we have shown that a deceleration of MSTID propagation velocities before the 2016 Kumamoto earthquake on April 15, 2016 has certainly occurred as candidate of *preseismic anomaly* behavior as reported by I&U17 (See Figure 2 of I&U17) and that the reduction of propagation velocities of MSTID as originally reported by I&U17 has been further clarified in comparison with the normal propagation velocity case of MSTID on April 13, 2016 (See Table S1 and Figures S17 to S29). Furthermore, we have provided three physical models (Models 1-3) to explain this abnormal deceleration of MSTID propagation veloci-
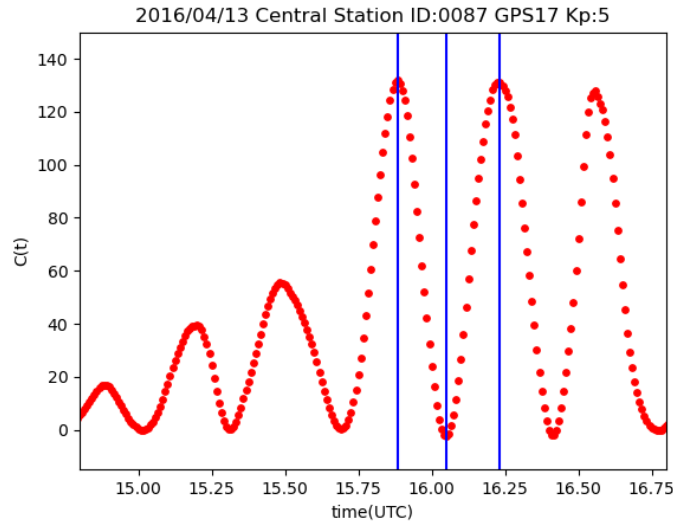
Figure 4. Correlation values (0087) on April 13, 2016
The vertical axis shows the correlation $C(T)$ and the horizontal one the time t (UTC).
The blue lines indicate the times t_1, t_2, t_3, $(t_1 < t_2 < t_3)$ when $C(T)$ has extremal values.
Because $\Delta T_1 \equiv t_2 - t_1 \simeq \Delta T_2 \equiv t_3 - t_2$, a deceleration of propagation velocity of MSTID
is not detectable. We used the pair of the GNSS station 0087 as a central station and
GPS satellite RRN17.
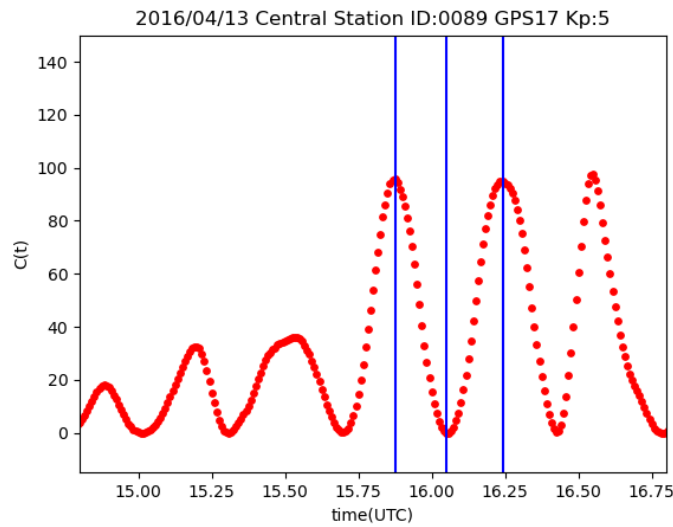
Figure 5. Correlation values (0089) on April 13, 2016
The vertical axis shows the correlation $C(T)$ and the horizontal one the time t (UTC).
The blue lines indicate the times t_1, t_2, t_3, $(t_1 < t_2 < t_3)$ when $C(T)$ has extremal values.
Because $\Delta T_1 \equiv t_2 - t_1 \simeq \Delta T_2 \equiv t_3 - t_2$, a deceleration of propagation velocity of MSTID
is not detectable. We used the pair of the GNSS station 0089 as a central station and
GPS satellite RRN17.

ties before large earthquakes. Interestingly, our estimation of 0.58 mV/m electric field requirement in the F-Layer ionosphere for 35 m/s deceleration of MSTID propagation velocities is almost consistent with Kelley's estimation of 0.5 mV/m electric field requirement at the base of ionosphere for dislocations of electrons firstly claimed by Heki (Kelley's et al., 2017; Heki, 2011; Muafiry and Heki, 2020; Heki, 2021). The $\times 10^4$ amplified effect with a measurement of MSITD propagation velocities elucidated in Section 3 is comparable with the amplified effect of CRA in increasing singal-to-noise-ratio introduced in Section 2. An electric field of 0.58 mV/m the of the F-Layer ionosphere is not detectable in practice, which means a high capability potential of ionospheric anomaly detection with TEC's CRA. There are other two physical models (Models 2-3) explaining deceleration of MSTID propagation velocities. Models 2-3 (decrease in Pedersen conductivity and increase in ion densities) are also consistent with DMSP satellite data of direct observations on O^+ prior to the 2011 Tohoku-Oki earthquake by Oyama et al. , 2019. By these physical models, one can argue that detected abnormality as deceleration at MSTID propagation velocities detected on the 2016 Kumamoto earthquake day is a *physical process* due to a sudden change of some physical parameters before the earthquake while there has been a missing link known as LAI coupling models (Pulinets and Ouzounov, 2011; Kuo, 2014). Concerning the 2011 Tohoku-Oki earthquake, various ionospheric anomaly phenomena have been reported so far (Heki, 2011; Kamiyama et. al. , 2016; Mizuno and Takashima, 2013; I&U16, Igarashi, et. al., 2020). Among them, Mizuno and Takashima, 2013, and Igarashi et al., 2020 observed some physical anomalies before the earthquake by direct measurement of physical parameters such as current in air and oblique ionograms between Wakkanai and Kokubunji in Japan, respectively. These indicated supportive physical evidences on the existence of certain abnormal preseismic phenomena before the Tohoku-Oki earthquake. In such a situation, Ikuta et al. 21 performed CRA analysis towards the Tohoku-Oki earthquake on March 11, 2011 and the foreshock on March 9, 2011. and reexamined I&U16. They reproduced CRA's high correlation value on March 11 of I&U16 and further argued that the correlation values $C(T)$ were not so abnormally high compared to the statistic of high $C(T)$ values such that $C(T) \geq 25$. (Fig. 2 of Ikuta et. al.). Again, the logic of the argument is based on the criteria of statistical anomaly values of Japan. Furthermore, the abnormality criteria should be taken by AND of various abnormality sensing detectors such as the low propagation velocity of MSTID and the low anomalous area rates as discussed in I&U17 while Ikuta et al. 21 considered these abnormality conditions separately. Moreover, because Earth's geomagnetic field strength on Tohoku area (higher latitude) is generally higher than Kumamoto area, ionospheric anomalies computed by $C(T)$ of Kumamoto (lower latitude) tend to be higher than Tohoku area (higher latitude). Thus, inconsistency on the threshold for abnormality criteria of $C(T)$ must exist between the case of 2011 Tohoku-Oki earthquake and the case of the 2016 Kumamoto earthquake.

Ikuta et. al. 21 claimed, however, that this high $C(T)$ anomaly would not be preseismic anomaly because of the inconsistency in that the 2011 Tohoku-Oki earthquake are not so large compared to $C(T)$ values of the 2016 Kumamoto earthquake. This argument would be true if preseismic ionospheric detectors should have a universal threshold of $C(T)$ for detecting earthquake anomaly. This is not true because of non-existence of such a universal threshold of $C(T)$ that must be dependent on the space and time of TEC observation data. This fact on the inconsistency of $C(T)$ is physical and already confirmed quantitatibly by extensive data analysis of CRA. Thus, the inconsistency cannot be used for the judgement of abnormality by CRA. Actually, $C(T)$ values have different values even for the same space and time zone if satellite orbits are different (Goto et al. 2019). With such inconsistency, a threshold of $C(T)$ can be computed by the mean and the variance of its preceding non-earthquake days such as 12 days.

Table 2. Maximum values of $C(T)$ of some days with Large Kp index in 2011 and 2016

Date	GPS(Station)	Kp	Max $C(T)$	t_{max} (UTC)	mean $C(T)$	sd in past 12 days	abnormality
2011/03/01	26(0214)	5	4.076	5.158	1.986	2.863	0.730
2011/03/01	5(0214)	5	8.203	4. 742	1.414	1.661	4.088
2011/03/11	26(0214)	5	24.674	5.675	1.108	1.314	17.928
2016/04/08	6(0087)	5	0.912	17.1	0.528	1.066	0.359
2016/04/08	17(0087)	5	3.974	15.567	0.932	1.439	2.113
2016/04/15	6(0087)	4	98.417	15.717	6.897	8.633	10.601
2016/04/15	17(0087)	4	34.353	16.158	6.585	7.789	3.565

Ikuta et al.21 also argued that the high value of $C(T)$ of the 2011 Tohoku-Oki earthquake may be attributed to the large Kp index and thus the anomaly detected (high $C(T)$ before the Tohoku-Oki earthquake) by CRA in I&U16 may be due to high-geomagnetic activity (Kp=5) . One can easily disprove the argument by Ikuta et.al. 21 by giving a counter example on the non-earthquake days with low $C(T)$ value and Large Kp index. Such days with low $C(T)$ and large Kp (Kp=5) can be illustrated as March 1, 2011 and April 8, 2016 both of which are the non-earthquake days (See Table 2). The days with (Kp=5) have no abnormality in $C(T)$ as compared to the earthquake days (March 11, 2011 and April 15, 2016). In the data analysis for computing a mean value and the standard deviation of $C(t)$, the 12 consecutive days before the target date were used for each day. In that data, data with low elevation angle (one hour from the beginning and one hour to the end of TEC data observed) were discarded for CRA to avoid high $C(T)$ values due to the low elevation angle. With the result, a signature of large Kp index has no relation with high $C(T)$ of CRA which can detect synchronously anomaly with multiple GNSS stations while the high $C(T)$ on 2011/03/11 and 2016/04/15 may be related to the two large earthquakes (the 2011 Tohoku-Oki earthquake and the 2016 Kumamoto earthquake), respectively, thus could be considered as ionospheric preseismic anomalies. At least, one cannot deny by the argument by Ikuta et al. 21. that high $C(T)$ phenomena on 2011/03/11 and 2016/04/15 are preseismic anomalies.

As explained in Section 2, we can have more sensible detectors rather than just using a single GNSS station technique by increasing signal-to-noise ratio in sensing abnormality. We think that the most important thing for detecting good ionospheric anomalies is to understand physics with ionospheric anomaly. With three physical models to explain deceleration in MSTID propagation velocity, one can understand the physics of a candidate ionospheric preseismic behavior as discussed in Section 3. To conclude, contrary to the claim by Ikuta et al. 21, TEC's correlation anomalies detected by I&U16 and I&U17 already provided supporting evidences that physical preseismic anomalies really exist.

References

Eisenbeis, J., Occhipinti, G. (2021). The TEC enhancement before seismic events is an artifact, *J. Geophys. Space Phys.*, 126, doi:10.1029/2020JA028733.

Igarashi, K., Tsuchiya, T., and Umeno, K. (2020). Characteristics of anomalous radio propagation before and after the 2011 Tohoku-Oki earth-

quake as seen by oblique ionograms, *Open J. Earthquake Res.*, 9, 100-112, doi:10.4236/ojer.2020.92007.

Ikuta, R., Oba, R., Kiguchi, D., and Hisada, T. (2021). Reanalysis of the ionospheric total electron content anomalies around the 2011 Tohoku-Oki and 2016 Kumamoto earthquakes: Lack of a clear precursor of large earthquakes, a preprint submitted to *J. Geophys. Res. : Space Physics* in 2021.

Iwata, T., and Umeno, K. (2016). Correlation analysis for preseismic total electron content anomalies around the 2011 Tohoku-Oki earthquake, *J. Geophys. Space Phys.*, 121, 8969-8984, doi:10.1002/2016JA023036.

Iwata, T., and Umeno, K. (2017). Preseismic ionospheric anomalies detected before the 2016 Kumamoto earthquake. *J. Geophys. Space Phys.*, 122, 3602-3616, doi:10.1002/2017JA023921.

Heki, K.,(2011). Ionospheric electron enhancement preceding the 2011 Tohoku-Oki earthquake, *Geophys. Res. Lett.*, L17312, doi:10.1029/2011GL047908.

Heki, K., and Enomoto, Y. (2013). Preseismic ionospheric electron enhancements revisited, *J. Geophys. Res. Space Phys.*, 120, pp.7006-7020, doi:10.1002/jgra.50578.

Heki, K.,(2021). Ionospheric disturbances related to earthquakes, *Wiley/AGU Boo: Advances in Ionospheric Research: Current Understanding and Challenges*, doi:10.1002/9781119815617.ch21

Kamiyama, M., Sugito, M., Kuse, M., Schekotov, A., and Hayakawa, M. (2016). On the precursors to the 2011 Tohoku-Oki earthquake: Crustal movements and electromagnetic signatures, *Geomatis, Natural Hazards and Risk*, 7(2), 471–492.

Kamogawa, M., and Kakinami, Y. (2013). Is an ionospheric electron enhancement preceding the 2011 Tohoku-Oki earthquake a precursor? *J. Geophys. Space Phys.*, 118, 1751-1754, doi:10.1002/jgra.50118.

Kelly, M-C., Swartz, W-E., and Heki, K. (2017). Apparent ionospheric total electron content variations prior to major earthquakes due to electric fields created by tectonic stresses, *J. Geophys. Space Phys.*, 122, 6689-6695, doi:10.1002/2016JA023601.

Kuo, C. L., Lee, L. C., and Huba, J. D. (2014). An improved coupling model for the lithosphere-atmosphere-ionosphere system, *J. Geophys. Space Phys.*,119, 3189–3205, doi:10.1002/2013JA019392.

Maeda, K-I., (1977). Conductivity and drifts in the ionosphere, *J. Atmos. Terr. Phys.*, 39, 1041-1053.

Masci, F., Thomas, J. N., Villani, F., Secan, J. A., and Rivera, N. (2015). On the onset of ionospheric precursors 40 min before strong earthquakes, *J. Geophys. Res. Space Phys.*, 120, 1383-1393, doi:10.1002/2014JA020822.

Mizuno, A., and Takashima, K. (2013) Continuous measurement of current in air and possible relation with intense earthquake, *J. Electrostatics.*, 71,3, 529-532, doi:10.1016/j.elstat.2012.11.015

Muafiry, I-N., and Heki, K. (2020). 3-D Tomography of the ionospheric anomalies immediately before and after the 2011 Tohoku-Oki (Mw 9.0) Earthquake, *J. Geophys. Res. Space Phys.* , 125(10), doi:10.1029/2020JA027993.

Otsuka, Y., Kotake, N., Shiokawa, K., Ogawa, T., Tsugawa, T., and Saito, A. (2011). Statistical study of medium-scale traveling ionospheric disturbances observed with a GPS receiver network in Japan, in *Aeronomy of the Earth's Atmosphere and Ionosphere*, edited by M. A. Abdu and D. Pancheva, IAGA Special Sopron Book Series 2, Springer.

Oyama, K. I., Chen, C. H., Bankov, L., Minakshi, D., Ryu, K., Liu, J. H., and Liu, H. (2019). Precursor effect of March 11, 2011 off the coast of Tohoku earthquake on high and low latitude ionospheres and its possible disturbing mechanism, *Advances in Space Research*, doi:10.1016/j.asr.2018.12.042

313   Perkins, F., (1973). Spread F and ionospheric currents, *J. Geophys. Res.*, 78, 218-
314   226, doi:10.1029/JA078i001p00218.
315   Pulinets, S., and Ouozounov, D. (2011). Lithosphere-Atmosphere-Ionosphere cou-
316   pling (LAIC) model- A unified concept for earthquake precursors validation, *J.*
317   *Asian Earth Sci.*, 41(4), 371–382.
318   Spitzer, L. (1962). *Physics of Fully Ionized Gases*,(John Wiley and Sons, 1962).

Supporting Information for "Capability of TEC correlation analysis and deceleration at propagation velocities of MSTID: Preseismic ionospheric anomalies before the large earthquakes"

Ken Umeno[1], Ryo Nakabayashi[1], Takuya Iwata[1], Minghui Kao[1]

[1] Department of Applied Mathematics and Physics, Graduate School of Informatics, Kyoto University, Kyoto, Japan

Contents of this file

1. Figures S1 to S29

2. Table S1

Additional Supporting Information (Files uploaded separately)

1. Captions for Movies S1 and S2

Introduction

Supplementary materials are composed of twenty nine Figures, two Movies, and one Table that help readers understand the manuscript better.

Figure S1 shows the locations of the fifteen GNSS stations used for TEC CoRelation Analysis (CRA) on April 13, 2021 and April 15, 2021 (the day of main shock of the 2016 Kumamoto earthquake).

———

July 24, 2021, 10:56pm

Figure S2 and Figure S3 show the correlation values at all the GNSS stations in Japan before the 2016 Kumamoto earthquake on 2016/04/15 (UTC) and on 2016/0413 (UTC), respectively.

Figures S4 to S16 show the correlation values for each different central station before the 2016 Kumamoto earthquake April 15, 2016 (UTC).

Figures S17 to S29 show the correlation values for each different central station on April 13, 2016 (UTC).

Movie S1 and Movie S2 show the temporal behavior of $C(T)$ on 2016/0415 (UTC) and on 2016/04/13(UTC), respectively.

Table S1 shows the list of the half periods of MSTID on April 13, 2016 estimated by CRA.

Caption for Movie S1 Movie S1. Correlation values at all the GNSS stations in Japan before the 2016 Kumamoto earthquake during the time range of 14:00-17:00 (UTC) on 2016/04/15. We used every GNSS station as a central station and mapped the results into the Japan map. The GPS satellite PRN 17 is used here. The black x marks represents the epicenter. The earthquake occurrence time is 16:25 UTC on April 15, 2016.

Caption for Movie S2 Movie S2. Correlation values at all the GNSS stations in Japan before the 2016 Kumamoto earthquake during the time range of 14:00-17:00 (UTC) on 2016/04/13. We used every GNSS station as a central station and mapped the results into the Japan map. The GPS satellite PRN 17 is used here.
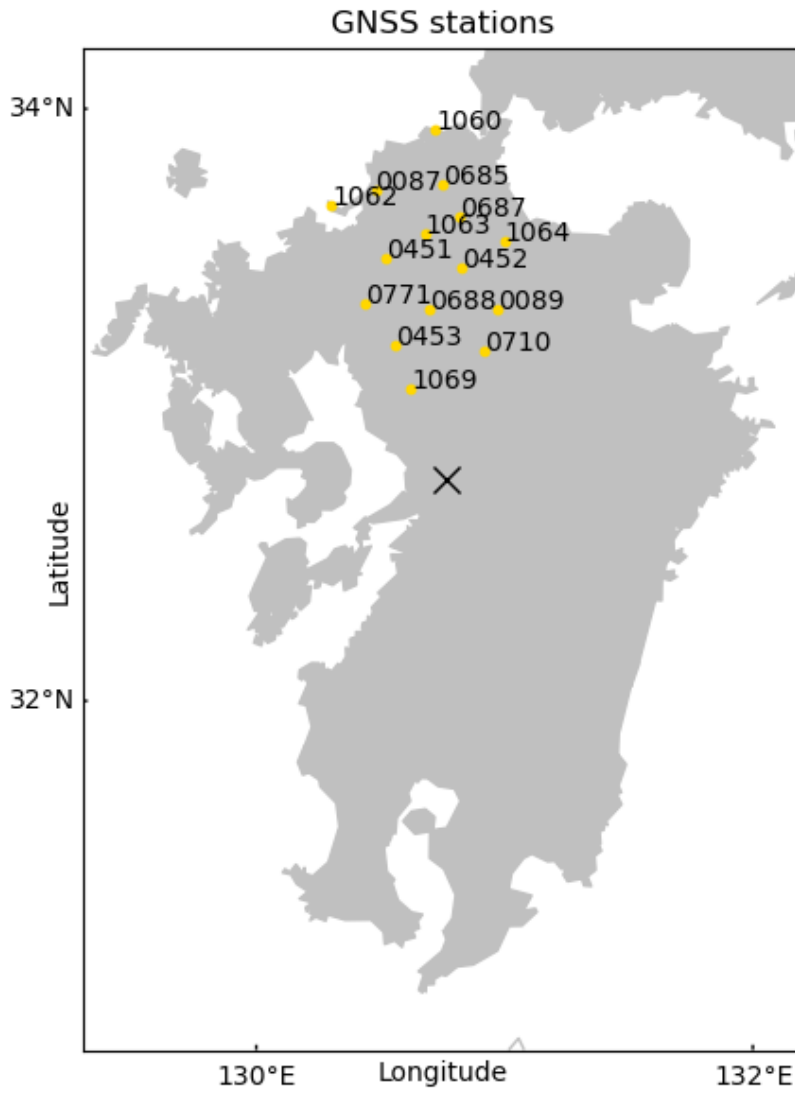
Figure S1. Location of the 15 selected GNSS stations for CRA
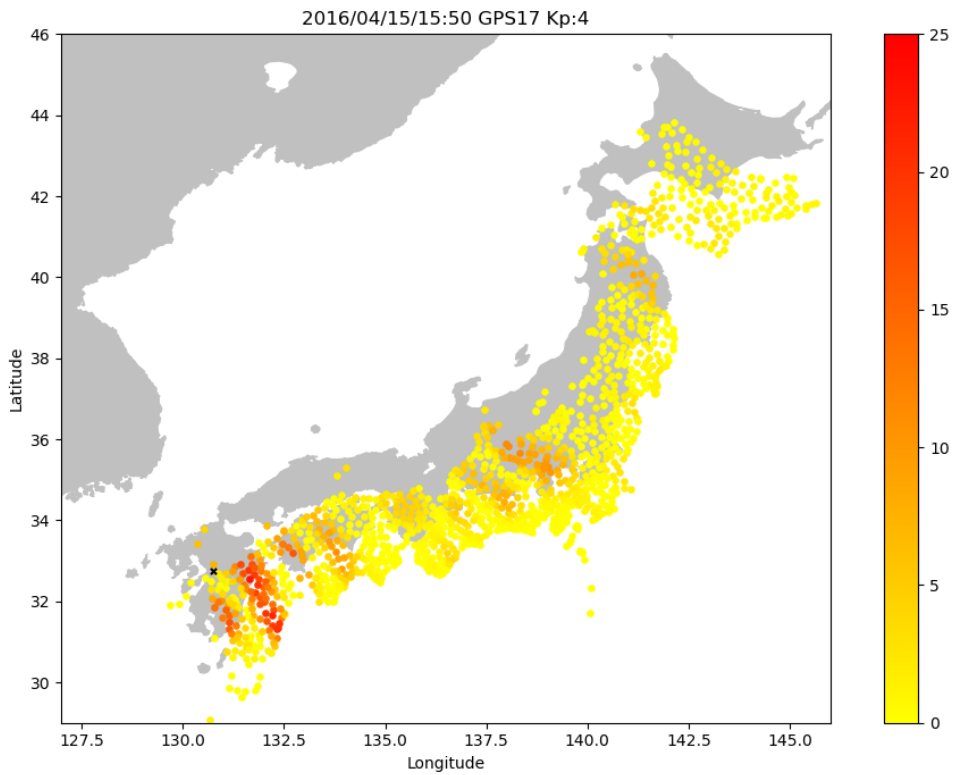
Figure S2. Correlation values at all the GNSS stations in Japan before the 2016 Kumamoto earthquake on 2016/04/15

We used every GNSS station as a central station and mapped the results into the Japan map. The GPS satellite PRN 17 is used here. The black x marks represents the epicenter. The earthquake occurrence time is 16:25 UTC on April 15, 2016 and the time 15:50 in the figure corresponds to 35 minutes before the main shock.
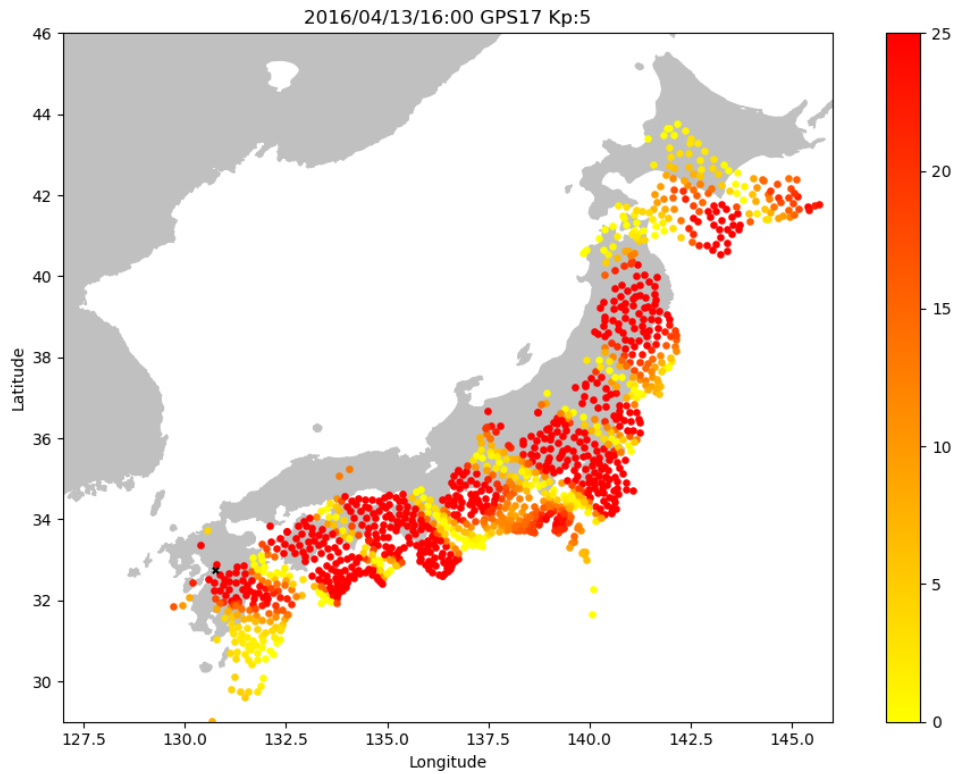
Figure S3. Correlation values at all the GNSS stations in Japan at 16:00 (UTC) on 2016/04/13. No earthquakes occurred on the day while MSTID was observed. We used every GNSS station as a central station and mapped the results onto the Japan map. The GPS satellite RRN17 is used here.

July 24, 2021, 10:56pm

:
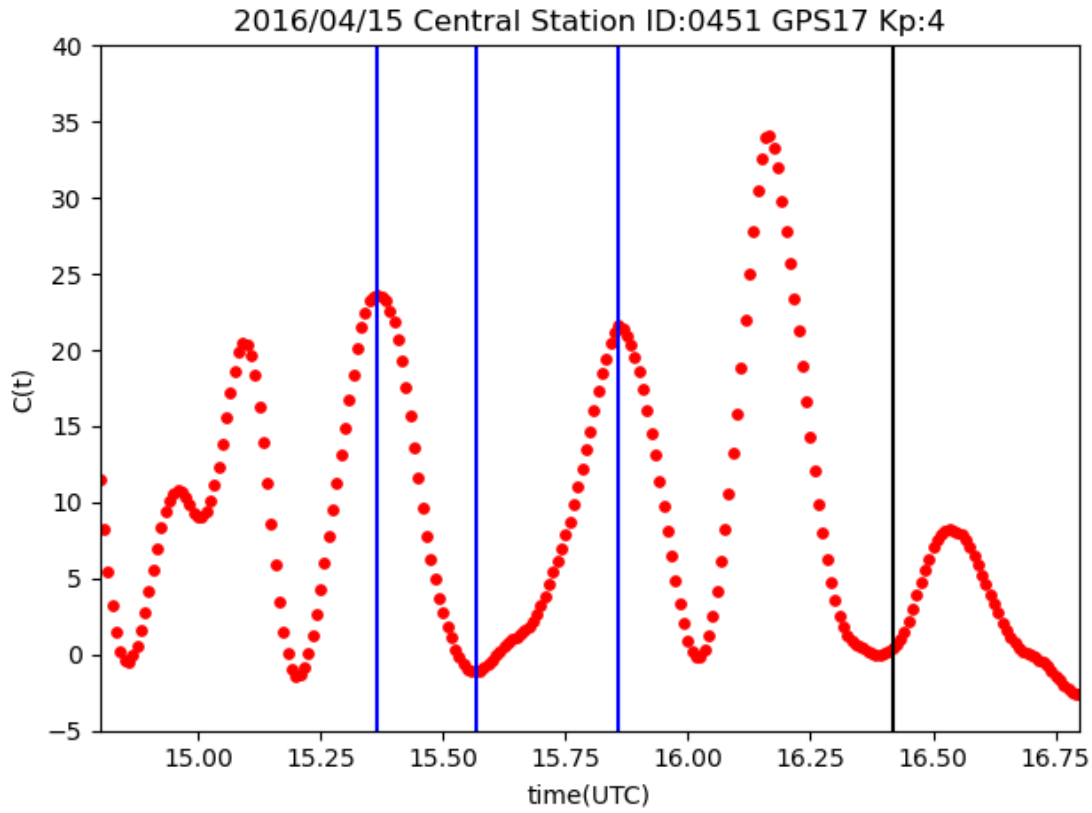
Figure S4. Correlation values before the 2016 Kumamoto earthquake (0451) on April 15, 2016

The vertical axis shows the correlation $C(T)$ and the horizontal one the time t (UTC). The black

line indicates the exact time 16:25 (UTC) when the 2016 Kumamoto earthquake occurred. The

blue lines indicate the times $t_1, t_2, t_3,\ (t_1 < t_2 < t_3)$ when $C(T)$ has extremal values. Because

$0 < \Delta T_1 \equiv t_2 - t_1 < \Delta T_2 \equiv t_3 - t_2$, a deceleration at propagation velocity of MSTID is clarified.

The GNSS station 0451 is used as the central station and the GPS satellite RRN17 is selected

for the analysis.
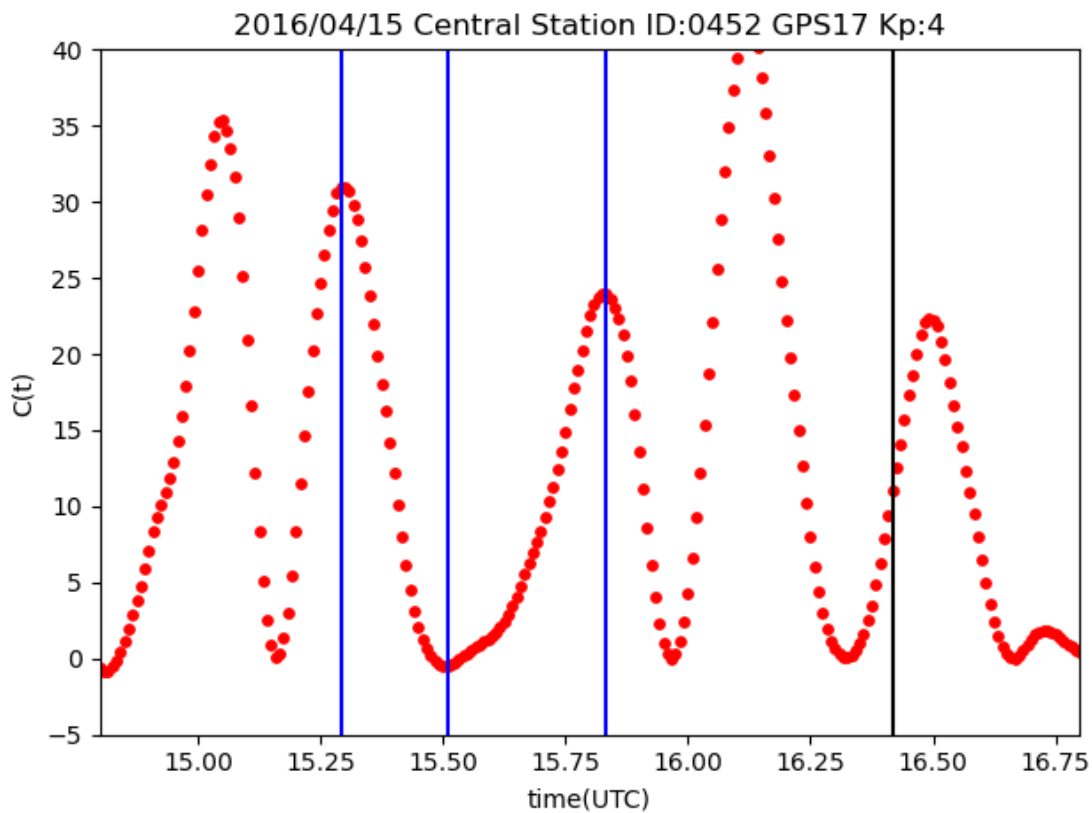
Figure S5. Correlation values before the 2016 Kumamoto earthquake (0452) on April 15, 2016

The vertical axis shows the correlation $C(T)$ and the horizontal one the time t (UTC). The black

line indicates the exact time 16:25 (UTC) when the 2016 Kumamoto earthquake occurred. The

blue lines indicate the times t_1, t_2, t_3, $(t_1 < t_2 < t_3)$ when $C(T)$ has extremal values. Because

$0 < \Delta T_1 \equiv t_2 - t_1 < \Delta T_2 \equiv t_3 - t_2$, a deceleration at propagation velocity of MSTID is clarified.

The GNSS station 0452 is used as the central station and the GPS satellite RRN17 is selected

for the analysis.

:
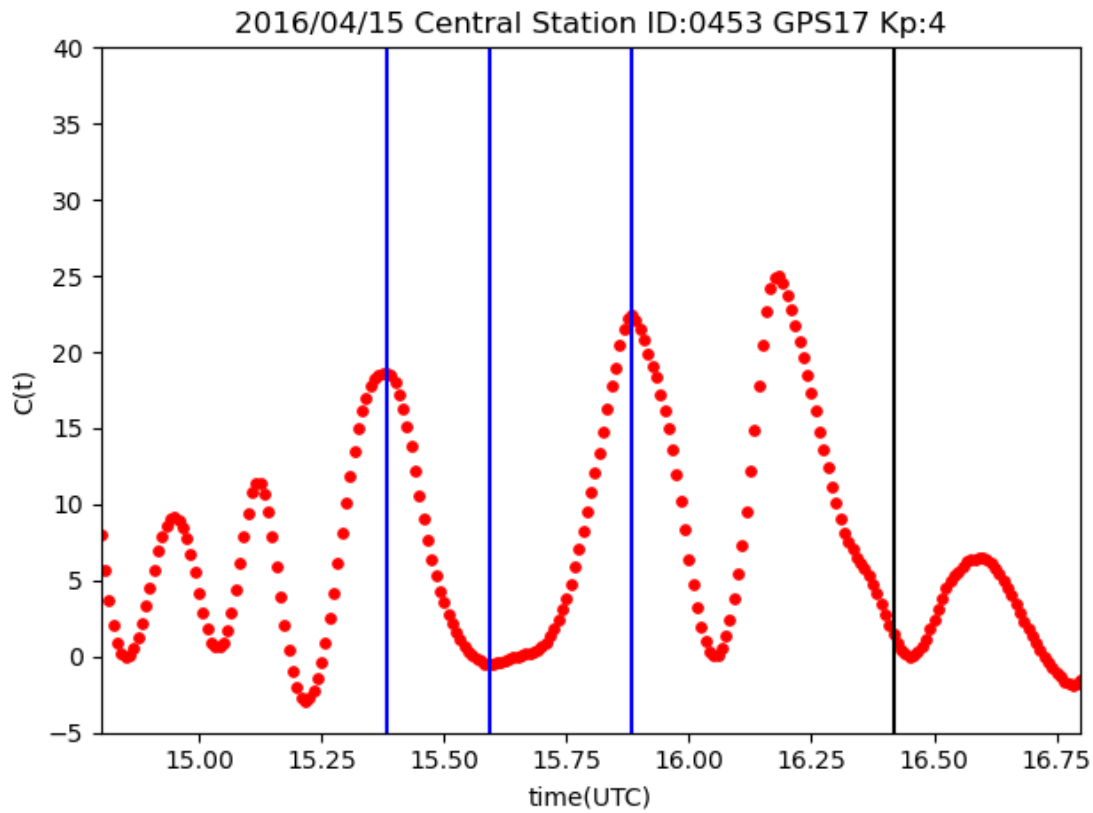
Figure S6. Correlation values before the 2016 Kumamoto earthquake (0453) on April 15, 2016

The vertical axis shows the correlation $C(T)$ and the horizontal one the time t (UTC). The black

line indicates the exact time 16:25 (UTC) when the 2016 Kumamoto earthquake occurred. The

blue lines indicate the times $t_1, t_2, t_3, \ (t_1 < t_2 < t_3)$ when $C(T)$ has extremal values. Because

$0 < \Delta T_1 \equiv t_2 - t_1 < \Delta T_2 \equiv t_3 - t_2$, a deceleration at propagation velocity of MSTID is clarified.

The GNSS station 0453 is used as the central station and the GPS satellite RRN17 is selected

for the analysis.
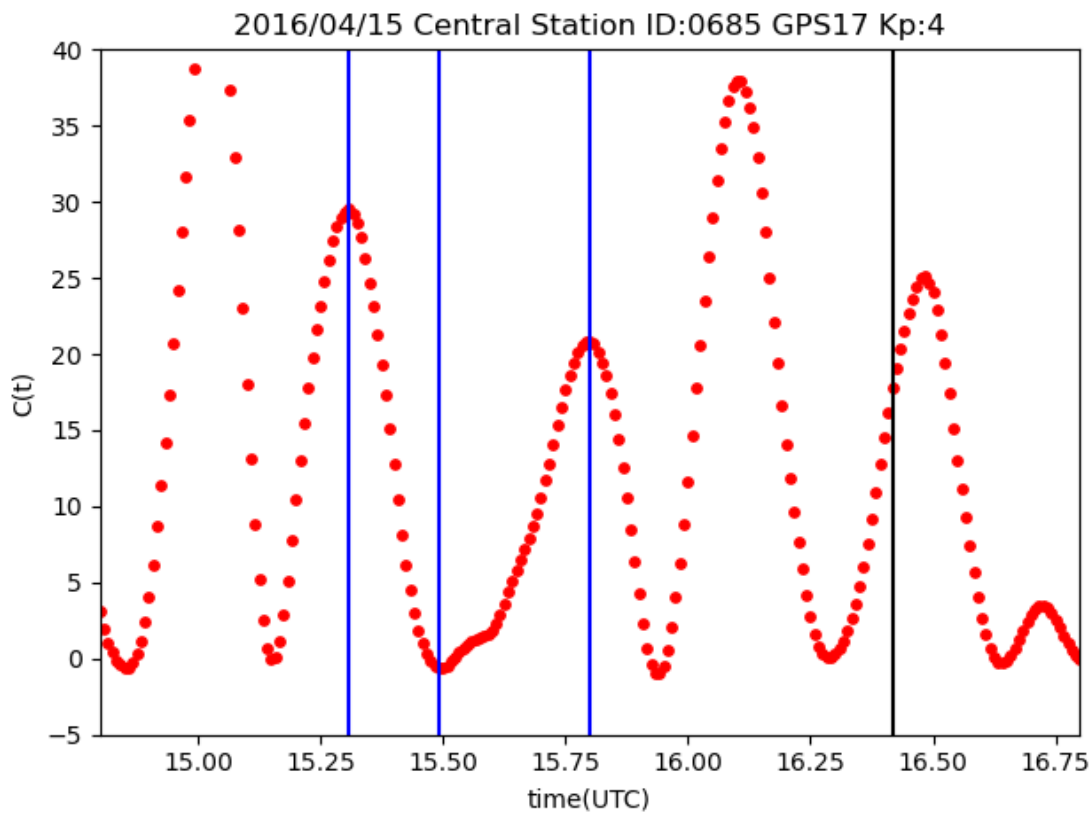
Figure S7.   Correlation values before the 2016 Kumamoto earthquake (0685) on April 15, 2016

The vertical axis shows the correlation $C(T)$ and the horizontal one the time t (UTC). The black

line indicates the exact time 16:25 (UTC) when the 2016 Kumamoto earthquake occurred. The

blue lines indicate the times $t_1, t_2, t_3, \ (t_1 < t_2 < t_3)$ when $C(T)$ has extremal values. Because

$0 < \Delta T_1 \equiv t_2 - t_1 < \Delta T_2 \equiv t_3 - t_2$, a deceleration at propagation velocity of MSTID is clarified.

The GNSS station 0685 is used as the central station and the GPS satellite RRN17 is selected

for the analysis.

:
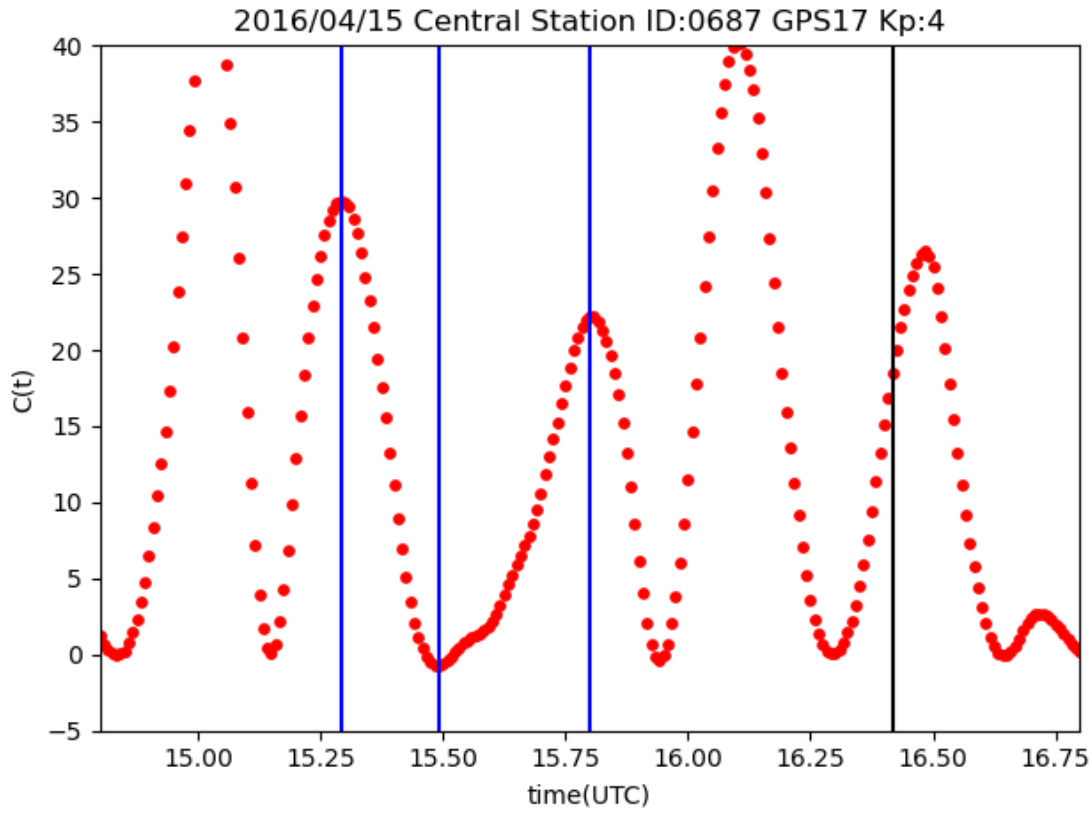
Figure S8. Correlation values before the 2016 Kumamoto earthquake (0687) on April 15, 2016

The vertical axis shows the correlation $C(T)$ and the horizontal one the time t (UTC). The black line indicates the exact time 16:25 (UTC) when the 2016 Kumamoto earthquake occurred. The blue lines indicate the times t_1, t_2, t_3, $(t_1 < t_2 < t_3)$ when $C(T)$ has extremal values. Because $0 < \Delta T_1 \equiv t_2 - t_1 < \Delta T_2 \equiv t_3 - t_2$, a deceleration at propagation velocity of MSTID is clarified. The GNSS station 0687 is used as the central station and the GPS satellite RRN17 is selected for the analysis.
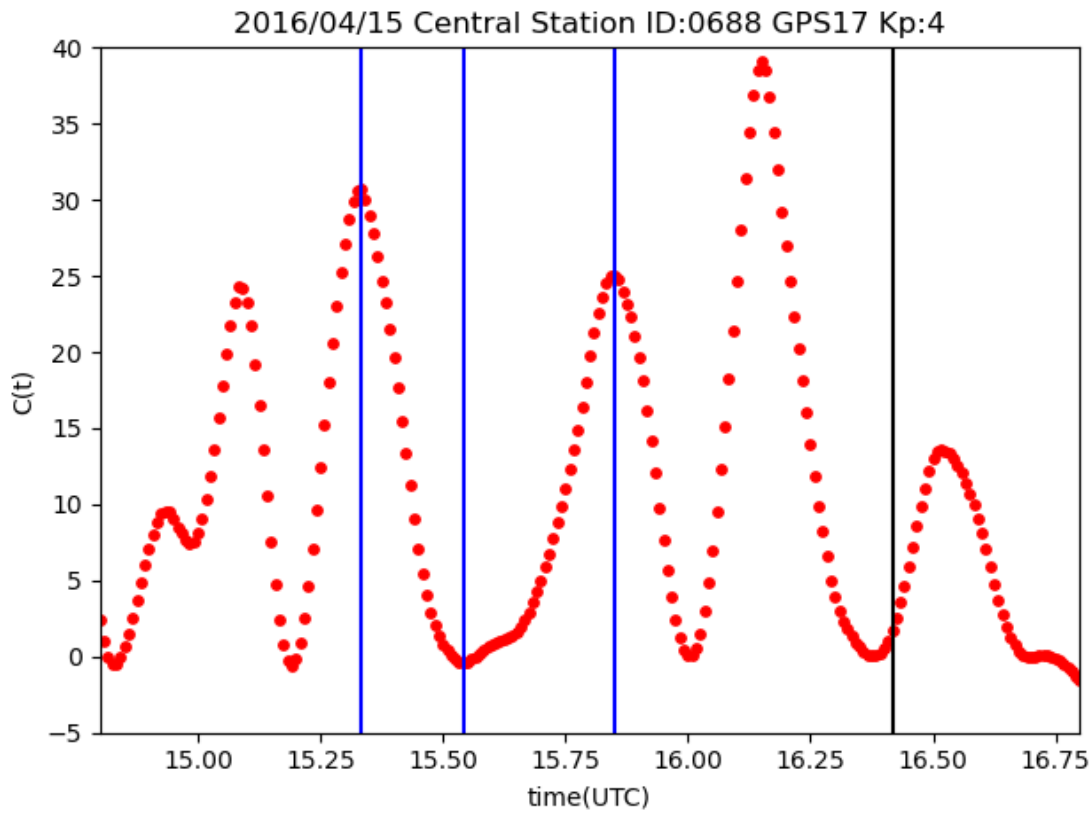
Figure S9. Correlation values before the 2016 Kumamoto earthquake (0688) on April 15, 2016

The vertical axis shows the correlation $C(T)$ and the horizontal one the time t (UTC). The black

line indicates the exact time 16:25 (UTC) when the 2016 Kumamoto earthquake occurred. The

blue lines indicate the times t_1, t_2, t_3, $(t_1 < t_2 < t_3)$ when $C(T)$ has extremal values. Because

$0 < \Delta T_1 \equiv t_2 - t_1 < \Delta T_2 \equiv t_3 - t_2$, a deceleration at propagation velocity of MSTID is clarified.

The GNSS station 0688 is used as the central station and the GPS satellite RRN17 is selected

for the analysis.
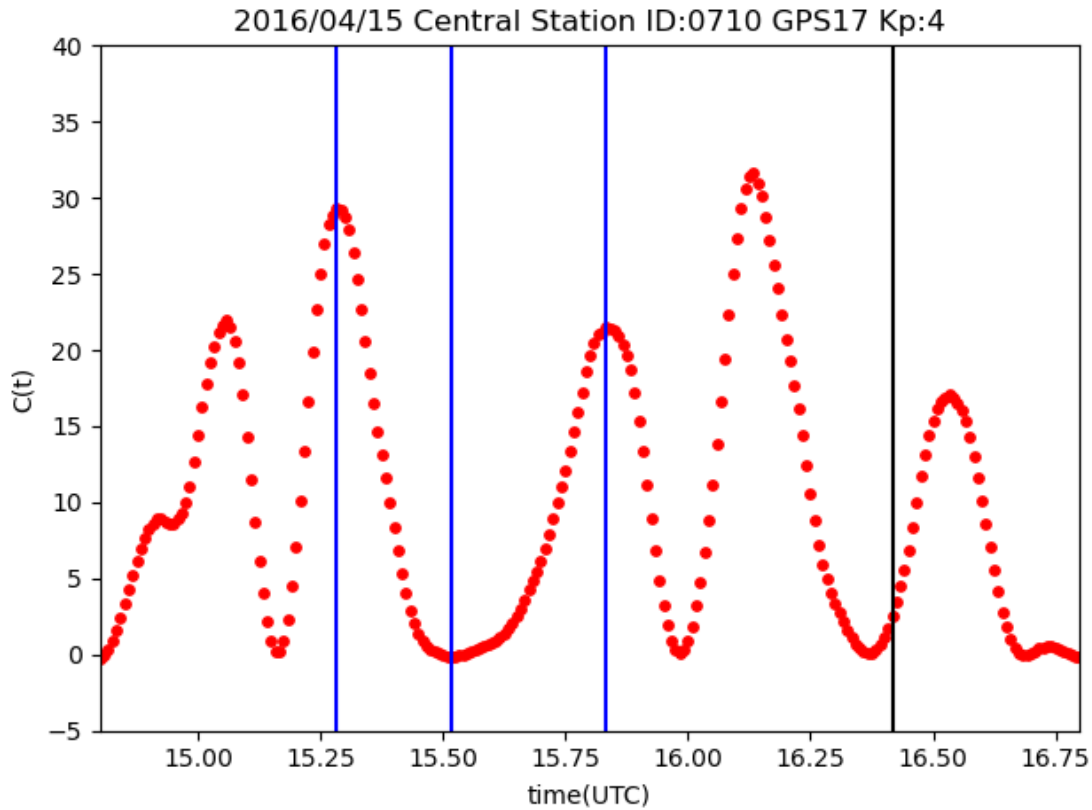
Figure S10. Correlation values before the 2016 Kumamoto earthquake (0710) on April 15, 2016

The vertical axis shows the correlation $C(T)$ and the horizontal one the time t (UTC). The black line indicates the exact time 16:25 (UTC) when the 2016 Kumamoto earthquake occurred. The blue lines indicate the times $t_1, t_2, t_3,\ (t_1 < t_2 < t_3)$ when $C(T)$ has extremal values. Because $0 < \Delta T_1 \equiv t_2 - t_1 < \Delta T_2 \equiv t_3 - t_2$, a deceleration at propagation velocity of MSTID is clarified. The GNSS station 0710 is used as the central station and the GPS satellite RRN17 is selected for the analysis.
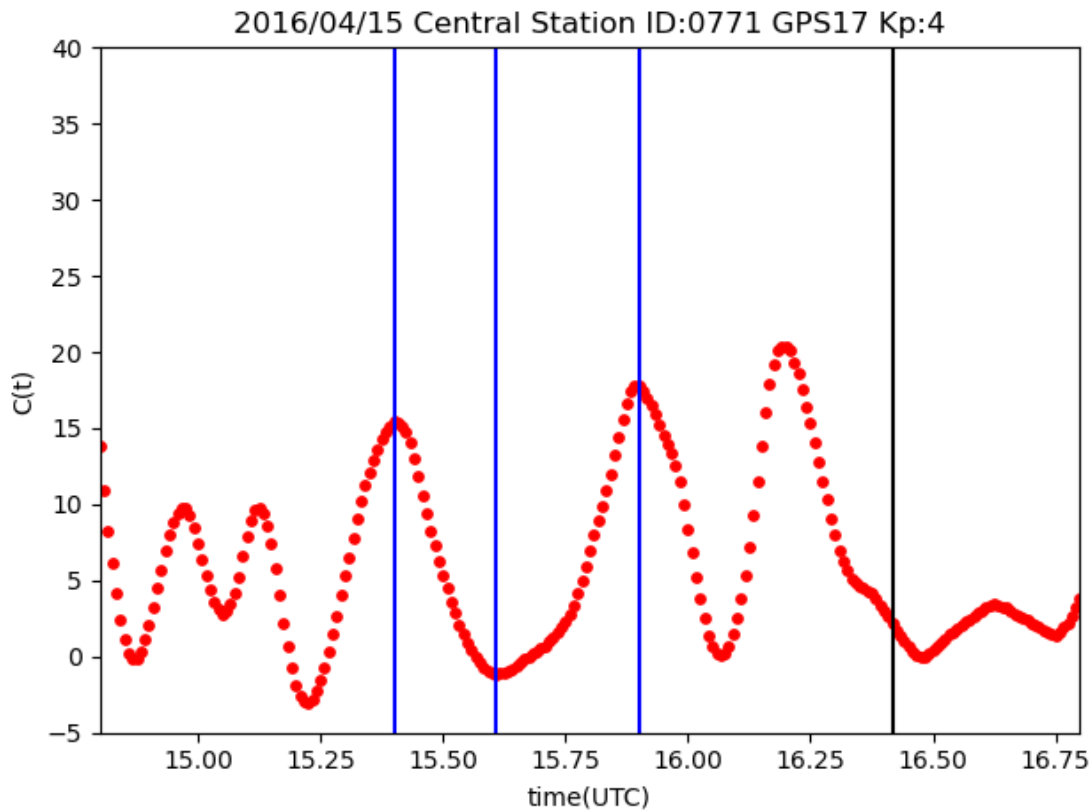
Figure S11. Correlation values before the 2016 Kumamoto earthquake (0711) on April 15, 2016

The vertical axis shows the correlation $C(T)$ and the horizontal one the time t (UTC). The black line indicates the exact time 16:25 (UTC) when the 2016 Kumamoto earthquake occurred. The blue lines indicate the times t_1, t_2, t_3, $(t_1 < t_2 < t_3)$ when $C(T)$ has extremal values. Because $0 < \Delta T_1 \equiv t_2 - t_1 < \Delta T_2 \equiv t_3 - t_2$, a deceleration at propagation velocity of MSTID is clarified. The GNSS station 0711 is used as the central station and the GPS satellite RRN17 is selected for the analysis.
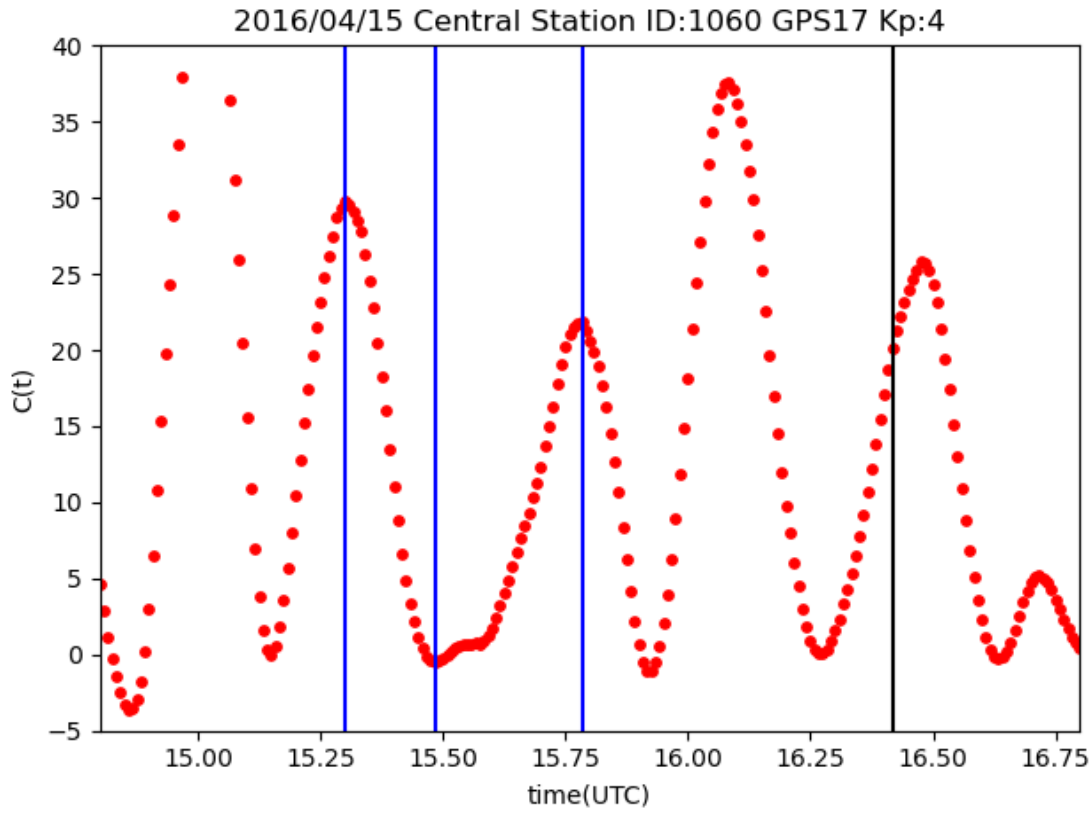
Figure S12. Correlation values before the 2016 Kumamoto earthquake (1060) on April 15, 2016

The vertical axis shows the correlation $C(T)$ and the horizontal one the time t (UTC). The black line indicates the exact time 16:25 (UTC) when the 2016 Kumamoto earthquake occurred. The blue lines indicate the times t_1, t_2, t_3, $(t_1 < t_2 < t_3)$ when $C(T)$ has extremal values. Because $0 < \Delta T_1 \equiv t_2 - t_1 < \Delta T_2 \equiv t_3 - t_2$, a deceleration at propagation velocity of MSTID is clarified. The GNSS station 1060 is used as the central station and the GPS satellite RRN17 is selected for the analysis.
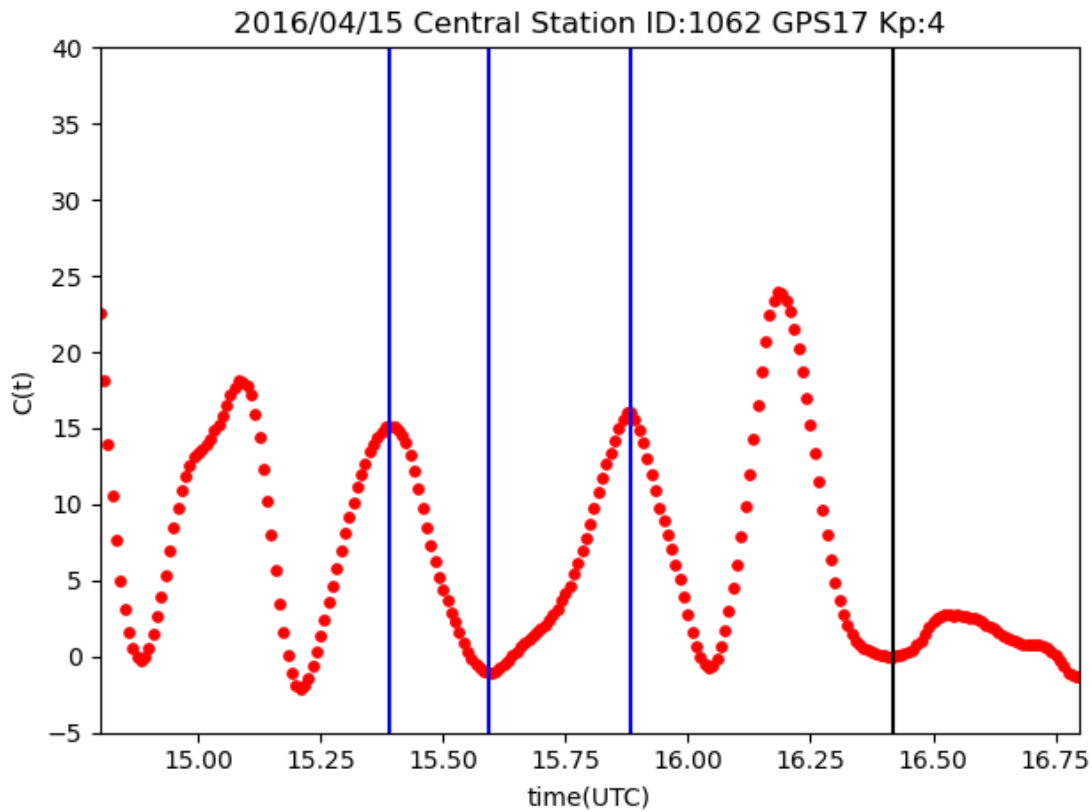
Figure S13. Correlation values before the 2016 Kumamoto earthquake (1062) on April 15, 2016

The vertical axis shows the correlation $C(T)$ and the horizontal one the time t (UTC). The black line indicates the exact time 16:25 (UTC) when the 2016 Kumamoto earthquake occurred. The blue lines indicate the times $t_1, t_2, t_3,\ (t_1 < t_2 < t_3)$ when $C(T)$ has extremal values. Because $0 < \Delta T_1 \equiv t_2 - t_1 < \Delta T_2 \equiv t_3 - t_2$, a deceleration at propagation velocity of MSTID is clarified. The GNSS station 1062 is used as the central station and the GPS satellite RRN17 is selected for the analysis.
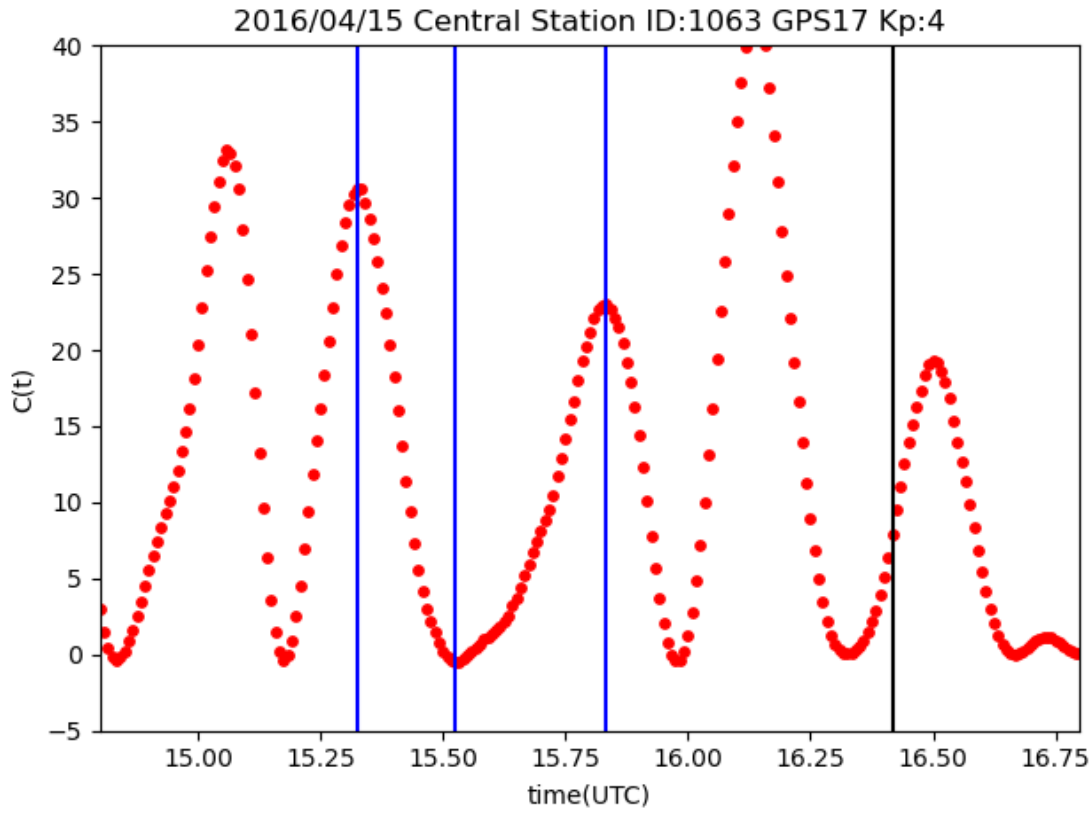
Figure S14.   Correlation values before the 2016 Kumamoto earthquake (1063) on April 15, 2016

The vertical axis shows the correlation $C(T)$ and the horizontal one the time t (UTC). The black line indicates the exact time 16:25 (UTC) when the 2016 Kumamoto earthquake occurred. The blue lines indicate the times $t_1, t_2, t_3, \ (t_1 < t_2 < t_3)$ when $C(T)$ has extremal values. Because $0 < \Delta T_1 \equiv t_2 - t_1 < \Delta T_2 \equiv t_3 - t_2$, a deceleration at propagation velocity of MSTID is clarified. The GNSS station 1063 is used as the central station and the GPS satellite RRN17 is selected for the analysis.
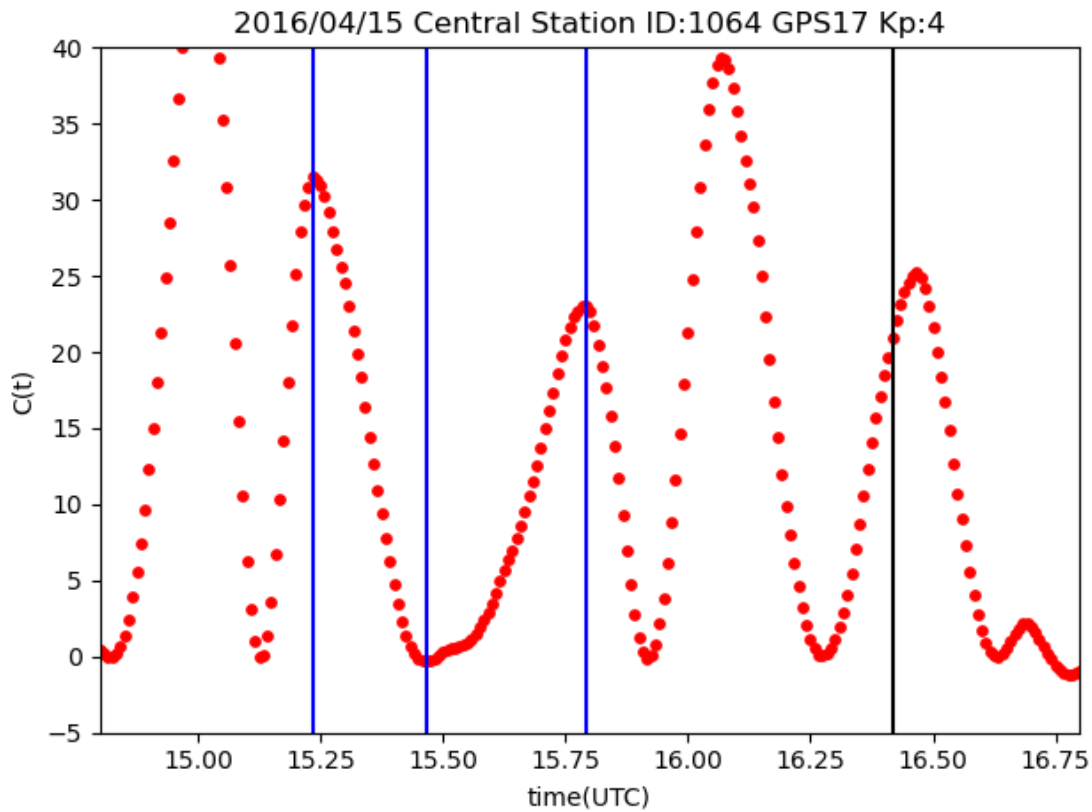
Figure S15. Correlation values before the 2016 Kumamoto earthquake (1064) on April 15, 2016

The vertical axis shows the correlation $C(T)$ and the horizontal one the time t (UTC). The black line indicates the exact time 16:25 (UTC) when the 2016 Kumamoto earthquake occurred. The blue lines indicate the times $t_1, t_2, t_3,$ $(t_1 < t_2 < t_3)$ when $C(T)$ has extremal values. Because $0 < \Delta T_1 \equiv t_2 - t_1 < \Delta T_2 \equiv t_3 - t_2$, a deceleration at propagation velocity of MSTID is clarified. The GNSS station 1064 is used as the central station and the GPS satellite RRN17 is selected for the analysis.
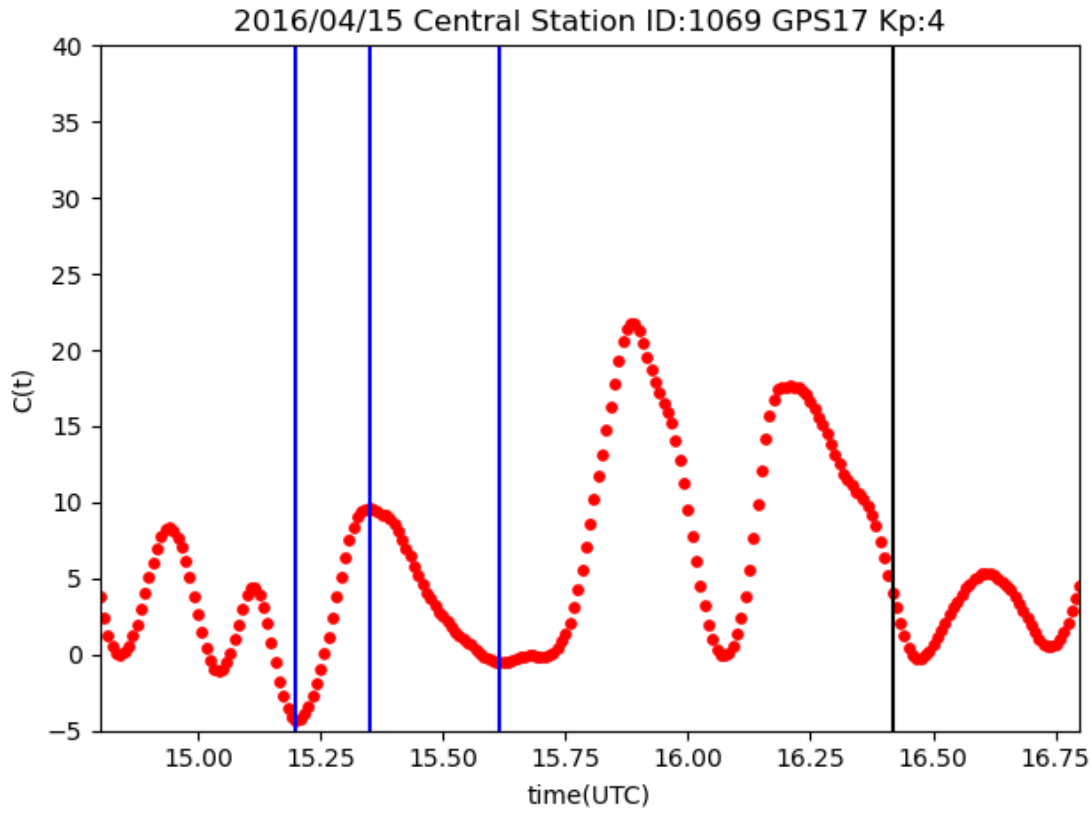
Figure S16.   Correlation values before the 2016 Kumamoto earthquake (1069) on April 15, 2016

The vertical axis shows the correlation $C(T)$ and the horizontal one the time t (UTC). The black line indicates the exact time 16:25 (UTC) when the 2016 Kumamoto earthquake occurred. The blue lines indicate the times $t_1, t_2, t_3,\ (t_1 < t_2 < t_3)$ when $C(T)$ has extremal values. Because $0 < \Delta T_1 \equiv t_2 - t_1 < \Delta T_2 \equiv t_3 - t_2$, a deceleration at propagation velocity of MSTID is clarified. The GNSS station 1069 is used as the central station and the GPS satellite RRN17 is selected for the analysis.
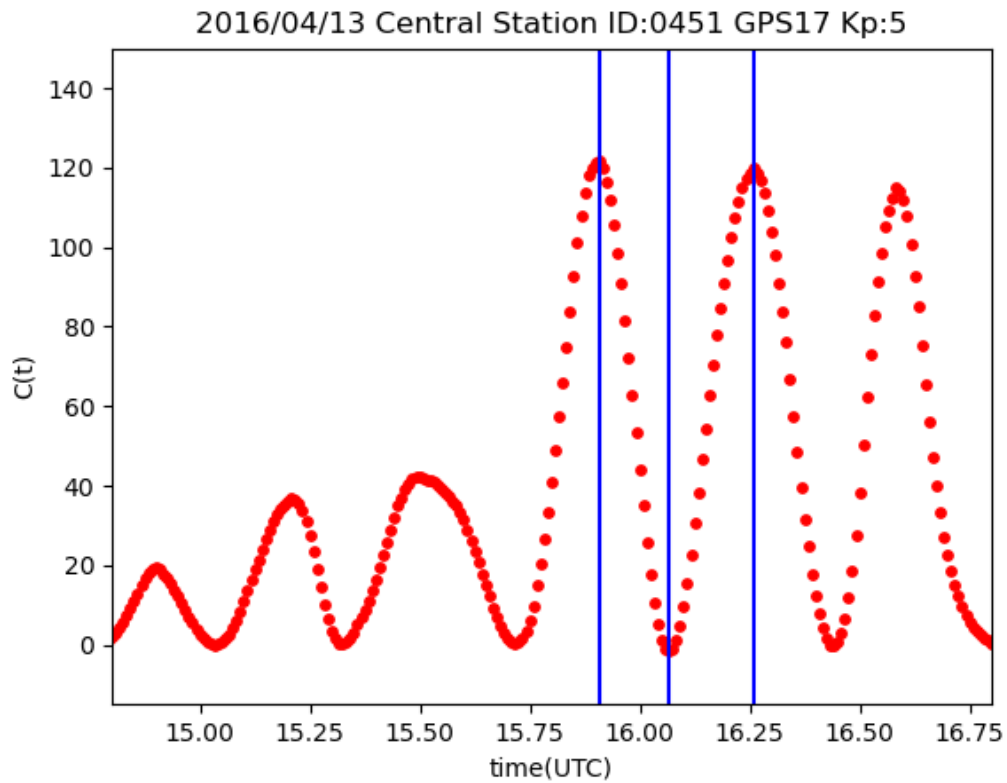
Figure S17. Correlation values (0451) on April 13, 2016

The vertical axis shows the correlation $C(T)$ and the horizontal one the time t (UTC). The blue lines indicate the times $t_1, t_2, t_3, \ (t_1 < t_2 < t_3)$ when $C(T)$ has extremal values. Because $\Delta T_1 \equiv t_2 - t_1 \simeq \Delta T_2 \equiv t_3 - t_2$, a deceleration of propagation velocity of MSTID is not detectable. We used the pair of the GNSS station 0451 as a central station and GPS satellite RRN17.

:
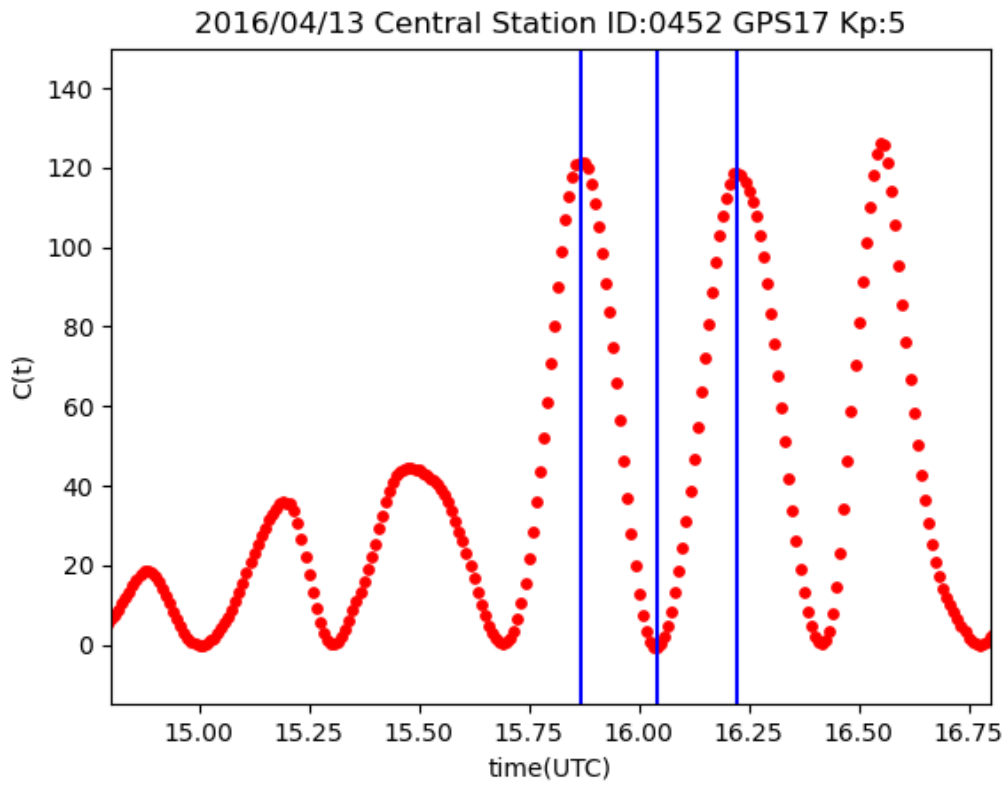
Figure S18. Correlation values (0452) on April 13, 2016

The vertical axis shows the correlation $C(T)$ and the horizontal one the time t (UTC). The blue lines indicate the times $t_1, t_2, t_3, \ (t_1 < t_2 < t_3)$ when $C(T)$ has extremal values. Because $\Delta T_1 \equiv t_2 - t_1 \simeq \Delta T_2 \equiv t_3 - t_2$, a deceleration of propagation velocity of MSTID is not detectable. We used the pair of the GNSS station 0452 as a central station and GPS satellite RRN17.
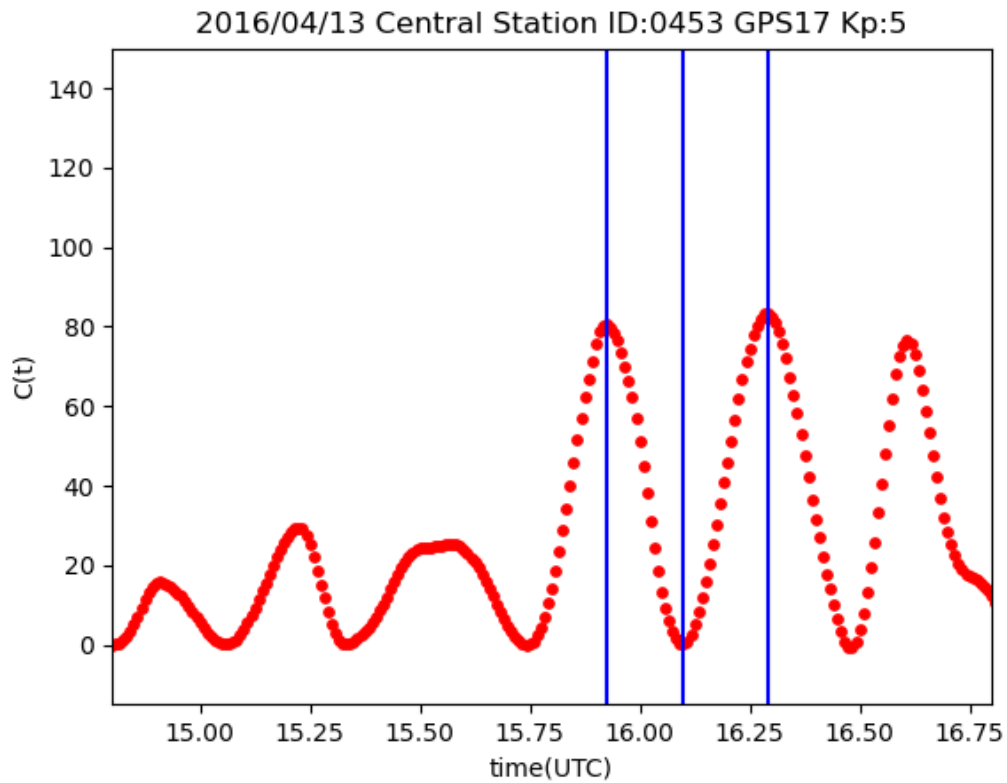
Figure S19. Correlation values (0453) on April 13, 2016

The vertical axis shows the correlation $C(T)$ and the horizontal one the time t (UTC). The blue lines indicate the times $t_1, t_2, t_3, \ (t_1 < t_2 < t_3)$ when $C(T)$ has extremal values. Because $\Delta T_1 \equiv t_2 - t_1 \simeq \Delta T_2 \equiv t_3 - t_2$, a deceleration of propagation velocity of MSTID is not detectable. We used the pair of the GNSS station 0453 as a central station and GPS satellite RRN17.
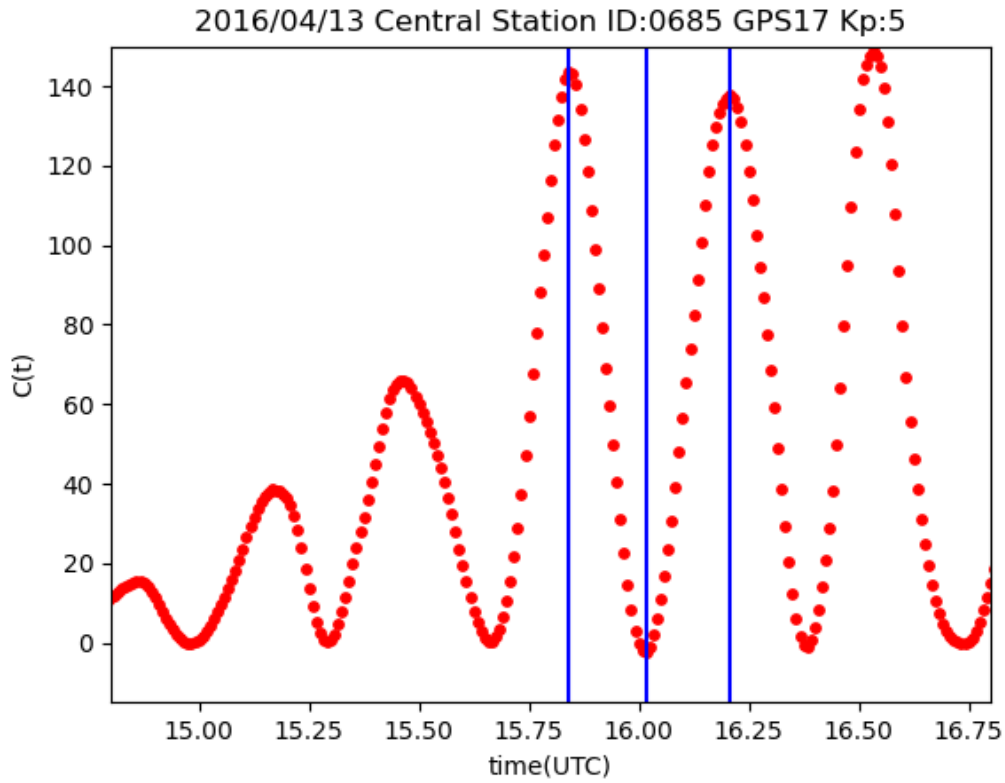
Figure S20. Correlation values (0685) on April 13, 2016

The vertical axis shows the correlation $C(T)$ and the horizontal one the time t (UTC). The blue lines indicate the times $t_1, t_2, t_3,\ (t_1 < t_2 < t_3)$ when $C(T)$ has extremal values. Because $\Delta T_1 \equiv t_2 - t_1 \simeq \Delta T_2 \equiv t_3 - t_2$, a deceleration of propagation velocity of MSTID is not detectable. We used the pair of the GNSS station 0685 as a central station and GPS satellite RRN17.
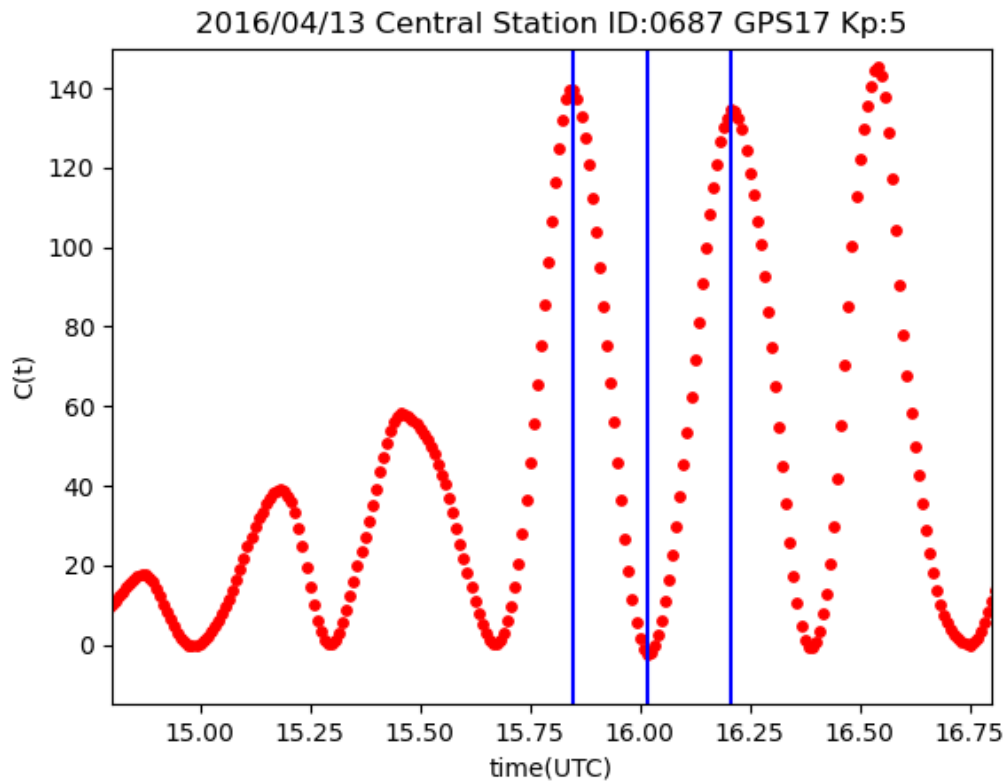
Figure S21. Correlation values (0687) on April 13, 2016

The vertical axis shows the correlation $C(T)$ and the horizontal one the time t (UTC). The blue lines indicate the times $t_1, t_2, t_3, \ (t_1 < t_2 < t_3)$ when $C(T)$ has extremal values. Because $\Delta T_1 \equiv t_2 - t_1 \simeq \Delta T_2 \equiv t_3 - t_2$, a deceleration of propagation velocity of MSTID is not detectable. We used the pair of the GNSS station 0687 as a central station and GPS satellite RRN17.

:
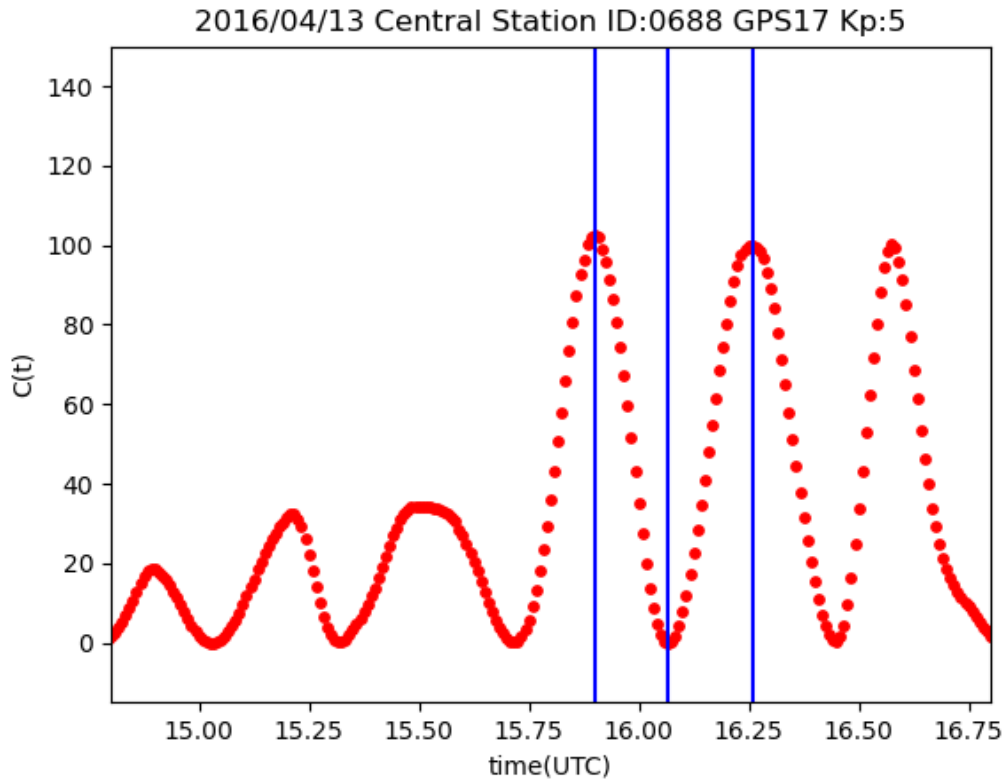
Figure S22. Correlation values (0688) on April 13, 2016

The vertical axis shows the correlation $C(T)$ and the horizontal one the time t (UTC). The blue lines indicate the times $t_1, t_2, t_3, \ (t_1 < t_2 < t_3)$ when $C(T)$ has extremal values. Because $\Delta T_1 \equiv t_2 - t_1 \simeq \Delta T_2 \equiv t_3 - t_2$, a deceleration of propagation velocity of MSTID is not detectable. We used the pair of the GNSS station 0688 as a central station and GPS satellite RRN17.

July 24, 2021, 10:56pm
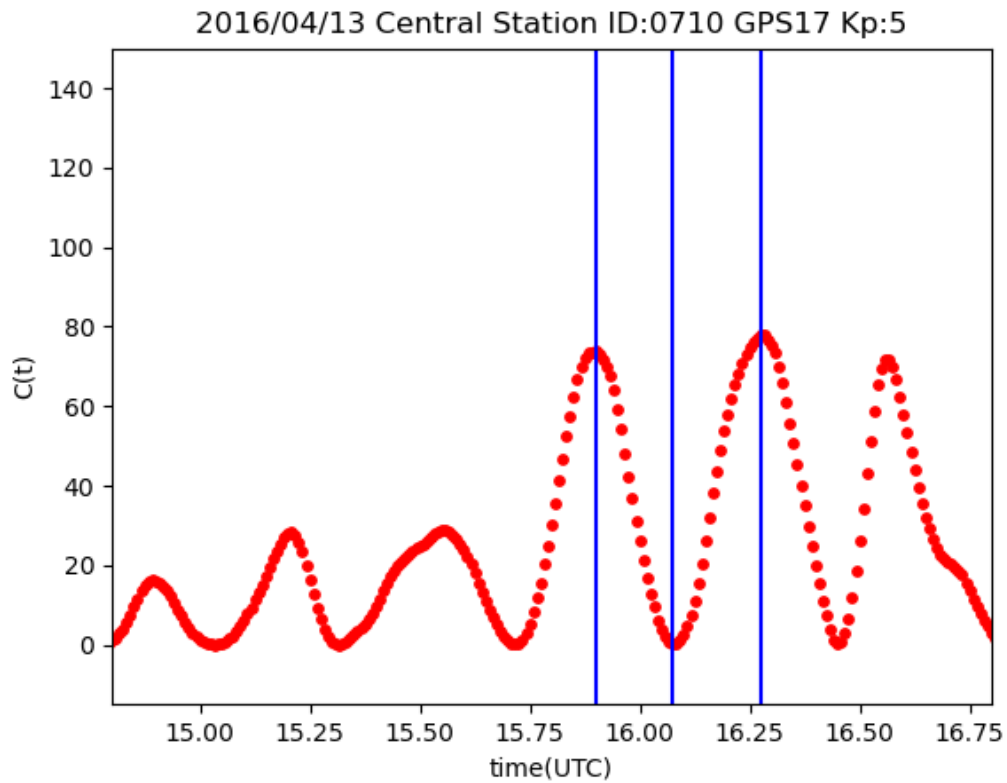
Figure S23. Correlation values (0710) on April 13, 2016

The vertical axis shows the correlation $C(T)$ and the horizontal one the time t (UTC). The blue lines indicate the times $t_1, t_2, t_3,$ $(t_1 < t_2 < t_3)$ when $C(T)$ has extremal values. Because $\Delta T_1 \equiv t_2 - t_1 \simeq \Delta T_2 \equiv t_3 - t_2$, a deceleration of propagation velocity of MSTID is not detectable. We used the pair of the GNSS station 0710 as a central station and GPS satellite RRN17.
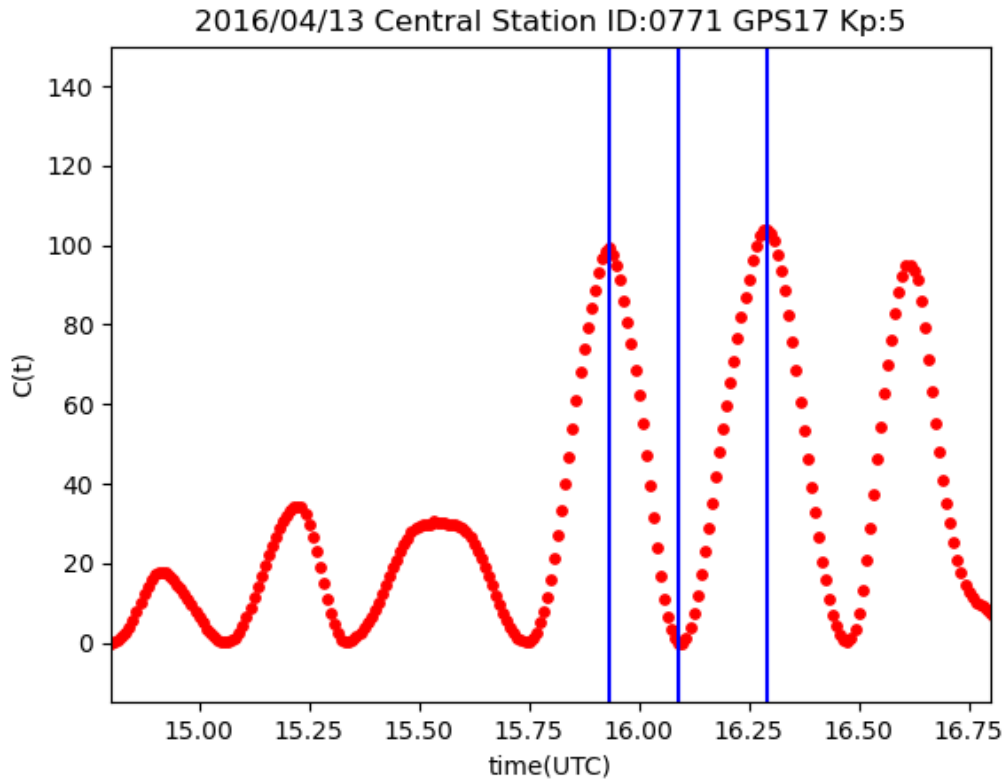
Figure S24. Correlation values (0771) on April 13, 2016

The vertical axis shows the correlation $C(T)$ and the horizontal one the time t (UTC). The blue lines indicate the times $t_1, t_2, t_3, \ (t_1 < t_2 < t_3)$ when $C(T)$ has extremal values. Because $\Delta T_1 \equiv t_2 - t_1 \simeq \Delta T_2 \equiv t_3 - t_2$, a deceleration of propagation velocity of MSTID is not detectable. We used the pair of the GNSS station 0771 as a central station and GPS satellite RRN17.
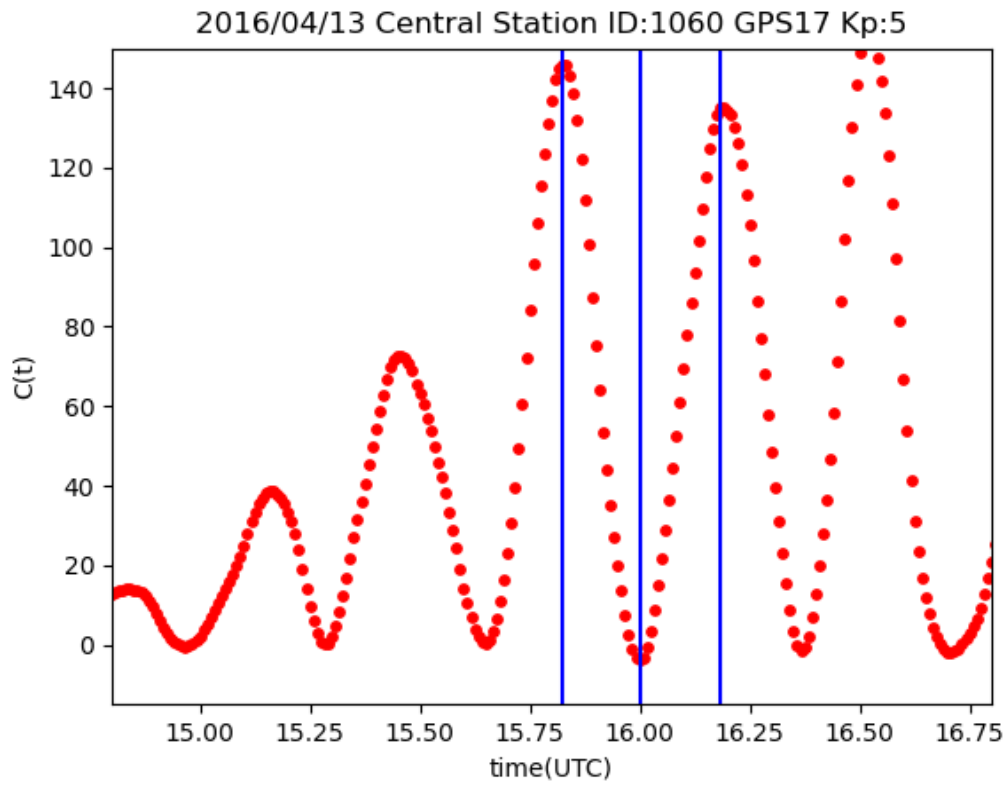
Figure S25. Correlation values (1060) on April 13, 2016

The vertical axis shows the correlation $C(T)$ and the horizontal one the time t (UTC). The blue lines indicate the times $t_1, t_2, t_3, \ (t_1 < t_2 < t_3)$ when $C(T)$ has extremal values. Because $\Delta T_1 \equiv t_2 - t_1 \simeq \Delta T_2 \equiv t_3 - t_2$, a deceleration of propagation velocity of MSTID is not detectable. We used the pair of the GNSS station 1060 as a central station and GPS satellite RRN17.

July 24, 2021, 10:56pm
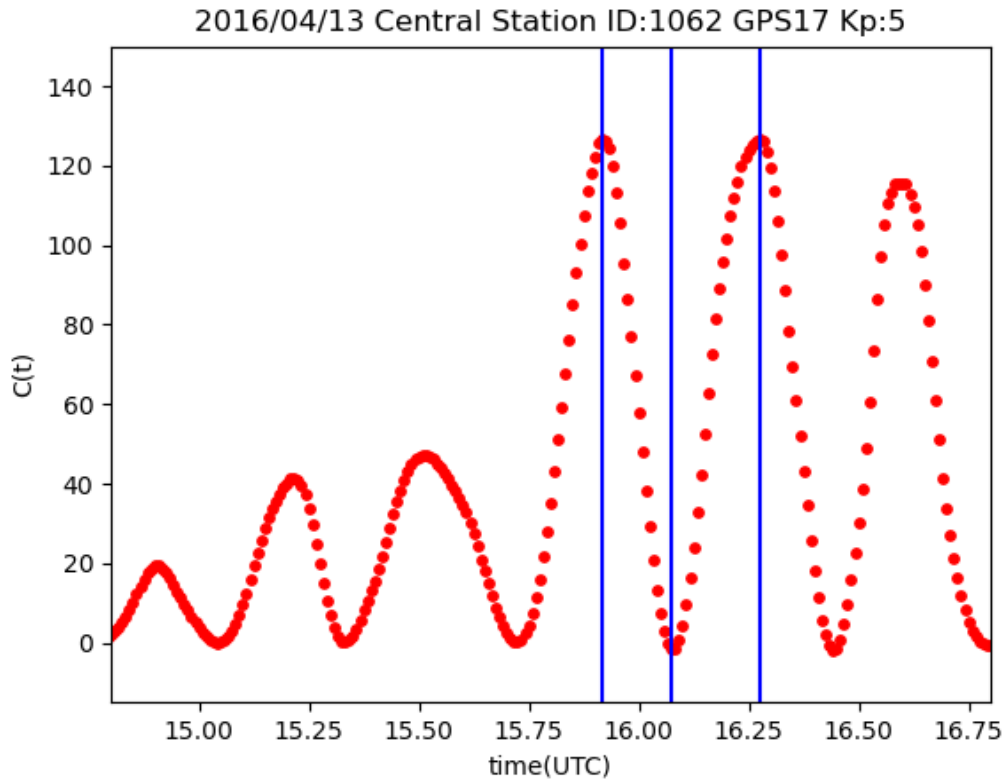
Figure S26. Correlation values (1062) on April 13, 2016

The vertical axis shows the correlation $C(T)$ and the horizontal one the time t (UTC). The blue lines indicate the times $t_1, t_2, t_3, \ (t_1 < t_2 < t_3)$ when $C(T)$ has extremal values. Because $\Delta T_1 \equiv t_2 - t_1 \simeq \Delta T_2 \equiv t_3 - t_2$, a deceleration of propagation velocity of MSTID is not detectable. We used the pair of the GNSS station 1062 as a central station and GPS satellite RRN17.

July 24, 2021, 10:56pm
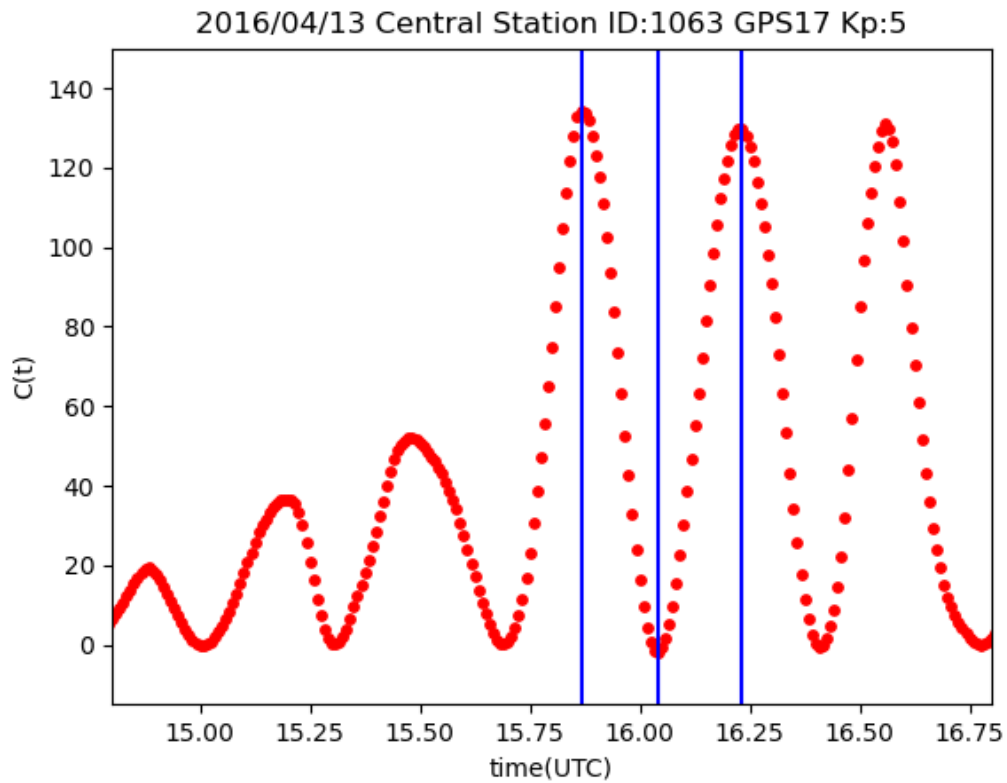
Figure S27. Correlation values (1063) on April 13, 2016

The vertical axis shows the correlation $C(T)$ and the horizontal one the time t (UTC). The blue lines indicate the times $t_1, t_2, t_3,$ $(t_1 < t_2 < t_3)$ when $C(T)$ has extremal values. Because $\Delta T_1 \equiv t_2 - t_1 \simeq \Delta T_2 \equiv t_3 - t_2$, a deceleration of propagation velocity of MSTID is not detectable. We used the pair of the GNSS station 1063 as a central station and GPS satellite RRN17.

:
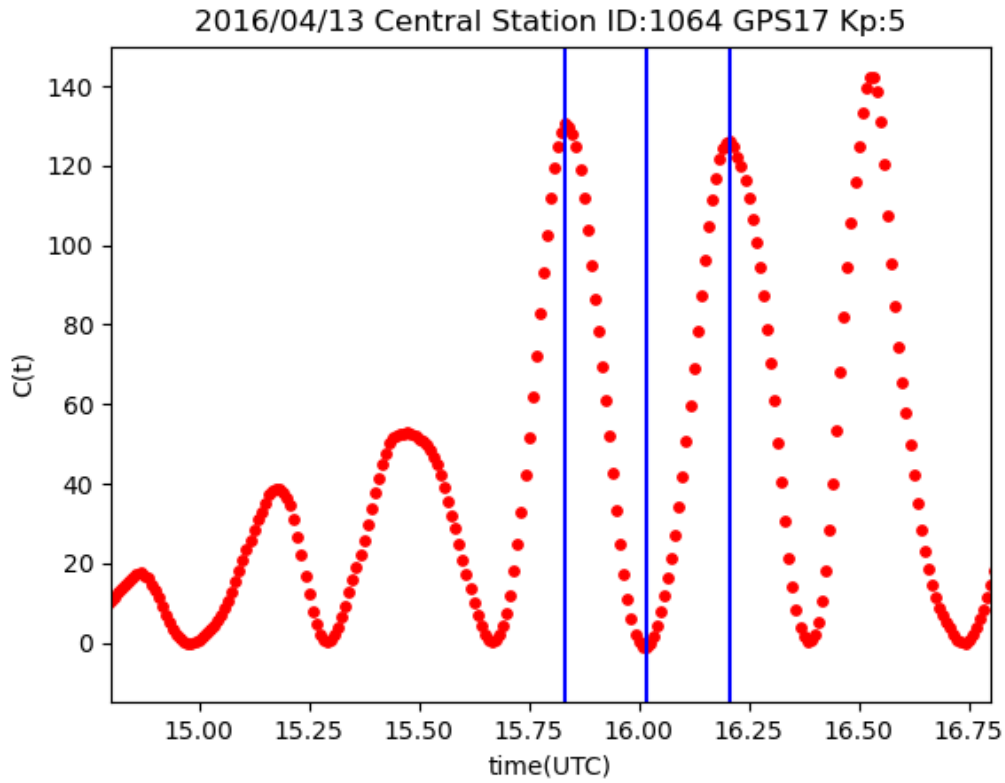
Figure S28. Correlation values (1064) on April 13, 2016

The vertical axis shows the correlation $C(T)$ and the horizontal one the time t (UTC). The blue lines indicate the times $t_1, t_2, t_3,\ (t_1 < t_2 < t_3)$ when $C(T)$ has extremal values. Because $\Delta T_1 \equiv t_2 - t_1 \simeq \Delta T_2 \equiv t_3 - t_2$, a deceleration of propagation velocity of MSTID is not detectable. We used the pair of the GNSS station 1064 as a central station and GPS satellite RRN17.
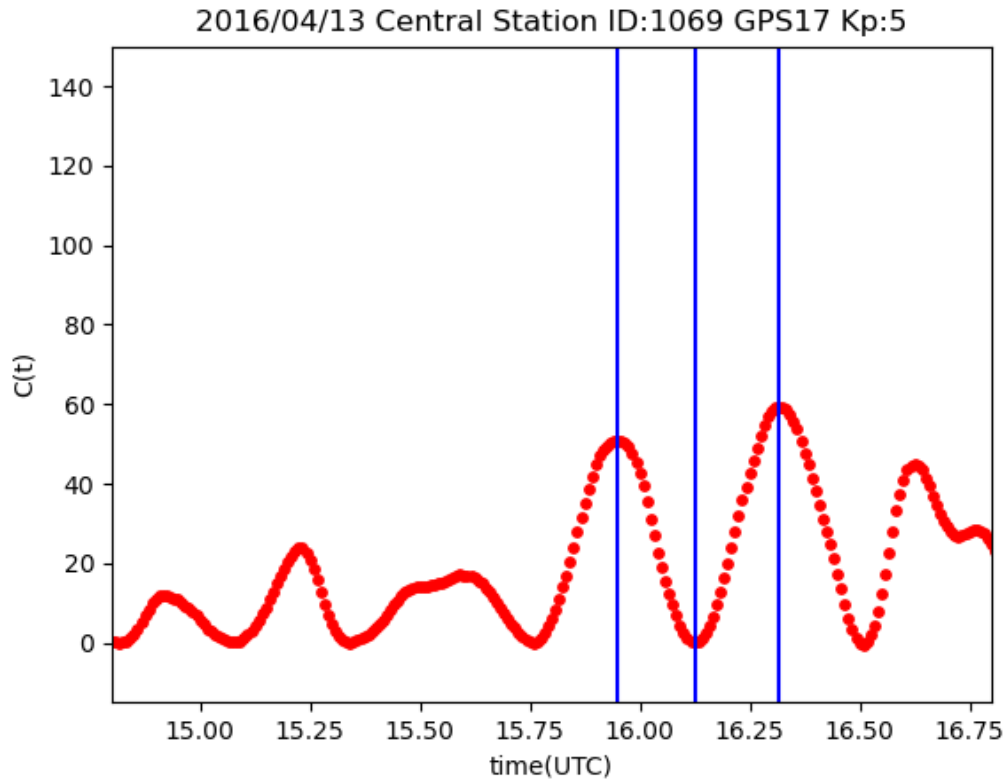
Figure S29. Correlation values (1069) on April 13, 2016

The vertical axis shows the correlation $C(T)$ and the horizontal one the time t (UTC). The blue lines indicate the times $t_1, t_2, t_3, \ (t_1 < t_2 < t_3)$ when $C(T)$ has extremal values. Because $\Delta T_1 \equiv t_2 - t_1 \simeq \Delta T_2 \equiv t_3 - t_2$, a deceleration of propagation velocity of MSTID is not detectable. We used the pair of the GNSS station 1069 as a central station and GPS satellite RRN17.

:

Table S1.   Half Periods of MSTIDs on April 13, 2016 Estimated by CRA

Station	ΔT_1 (hour)	ΔT_2 (hour)	Ratio $\gamma \left(\equiv \dfrac{\Delta T_1}{\Delta T_2} \right)$	t_1 (UTC)	t_2 (UTC)	t_3 (UTC)
0087	0.167	0.183	0.909	15.883	16.050	16.233
0089	0.175	0.192	0.913	15.875	16.050	16.242
0451	0.158	0.192	0.826	15.908	16.067	16.258
0452	0.175	0.183	0.955	15.867	16.042	16.225
0453	0.175	0.192	0.913	15.925	16.100	16.292
0685	0.175	0.192	0.913	15.842	16.017	16.208
0687	0.167	0.192	0.870	15.850	16.017	16.208
0688	0.167	0.192	0.870	15.900	16.067	16.258
0710	0.175	0.200	0.875	15.900	16.075	16.275
0771	0.158	0.200	0.792	15.933	16.092	16.292
1060	0.175	0.183	0.955	15.825	16.000	16.183
1062	0.158	0.200	0.792	15.917	16.075	16.275
1063	0.175	0.192	0.913	15.867	16.042	16.233
1064	0.183	0.192	0.957	15.833	16.017	16.208
1069	0.175	0.192	0.913	15.950	16.125	16.317